

PERFORMANCE ANALYSIS OF PHASE CHANGE MATERIAL INTEGRATED HEAT SINKS FOR THERMAL MANAGEMENT OF ELECTRONIC DEVICES

MS (Research) Thesis

By

PRADUNMYA PRAN DUTTA



DISCIPLINE OF MECHANICAL ENGINEERING
INDIAN INSTITUTE OF TECHNOLOGY INDORE

JUNE 2023

PERFORMANCE ANALYSIS OF PHASE CHANGE MATERIAL INTEGRATED HEAT SINKS FOR THERMAL MANAGEMENT OF ELECTRONIC DEVICES

A THESIS

*Submitted in fulfillment of the
requirements for the award of the degree
of*

Master of Science (Research)

by

PRADUNMYA PRAN DUTTA



**DISCIPLINE OF MECHANICAL ENGINEERING
INDIAN INSTITUTE OF TECHNOLOGY INDORE**

JUNE 2023



INDIAN INSTITUTE OF TECHNOLOGY INDORE

CANDIDATE'S DECLARATION

I hereby certify that the work which is being presented in the thesis entitled **PERFORMANCE ANALYSIS OF PHASE CHANGE MATERIAL INTEGRATED HEAT SINKS FOR THERMAL MANAGEMENT OF ELECTRONIC DEVICES** in the fulfillment of the requirements for the award of the degree of **MASTER OF SCIENCE (RESEARCH)** and submitted in the **Discipline of Mechanical Engineering, Indian Institute of Technology Indore**, is an authentic record of my own work carried out during the time period August 2021 to June 2023 under the supervision of **Dr. Santosh Kumar Sahu, Professor, Indian Institute of Technology Indore**.

The matter presented in this thesis has not been submitted by me for the award of any other degree of this or any other institute.

Pradunmya Pran Dutta
15/12/2023
Signature of the student
(Pradunmya Pran Dutta)

This is to certify that the above statement made by the candidate is correct to the best of my knowledge.

S.K.S. 15/12/2023
Signature of the Supervisor of
MS (Research) thesis
(Dr. Santosh Kr. Sahu)

Pradunmya Pran Dutta has successfully given his MS (Research) Oral Examination held on **15th December, 2023**.

Pradunmya Pran Dutta
15/12/2023
Signature of Chairperson (OEB)

S.K.S.
15/12/2023
Signature of Thesis Supervisor

Satyamraj 15/12/2023
Signature of Convener, DPGC

S.K.S.
Signature of Head of Discipline
15 DEC 2023

ACKNOWLEDGEMENTS

I would like to express my profound appreciation to Dr. Santosh Kumar Sahu, my supervisor from the Department of Mechanical Engineering at the Indian Institute of Technology Indore. His patient guidance, support, encouragement, and advice throughout my research work have been invaluable. I consider myself fortunate to have had a supervisor who demonstrated such care for my work and consistently responded promptly to my questions and inquiries. At various stages of this research project, I greatly benefited from his advice, particularly when exploring new ideas. Furthermore, his meticulous editing significantly contributed to the production of this thesis.

I extend my gratitude to PSPC members: Dr. Shanmugam Dhinakaran, Professor from the Department of Mechanical Engineering; and Dr. Prabhat Kumar Upadhyay, Professor from the Department of Electrical Engineering, both from the Indian Institute of Technology Indore. Their valuable suggestions and comments during this work are deeply appreciated. I am also thankful to the Head, DPGC convener, all faculty members, and staff of the Discipline of Mechanical Engineering for their timely assistance and support. I would like to acknowledge and show respect to Dr. Suhas Joshi, Director of the Indian Institute of Technology Indore, for providing me with the opportunity to explore my research capabilities at IIT Indore.

I am indebted to my seniors, lab mates, and fellow researchers, especially Mr. Vivek Saxena, Mr. Akhalesh Sharma, Dr. Anuj Kumar, Mr. Jay Joshi, Mr. Pawan Sharma, and Mr. Pradeep Singh, for their cooperation and camaraderie, which made my MS (R) journey a joyful and fulfilling experience. I extend my thanks to Mr. Arun Kumar Bhagwaniya from the Fluid Mechanics and Machinery Lab.

I would like to express my sincere respect to my grandparents and my parents for their unwavering love, care, and support throughout my life. I would like to give a special mention to my parents, whose support has been unwavering in every step of my life, from my childhood to my master's degree. Their constant support and encouragement throughout my academic career have played a pivotal role in helping me achieve my

goals. Special thanks are extended to my brother for his unwavering support and encouragement.

Finally, I am grateful to all who have directly or indirectly contributed, aided, and supported me on this journey.

-Pradunmya Pran Dutta

Dedicated to my family for their love, care, and blessings

Abstract

Present thesis reports the experimental investigations pertaining to the performance analysis of phase change material integrated heat sinks for thermal management of electronic devices.

Initially, an experimental investigation focuses on employing phase change material (PCM) based heat sinks for passive thermal management system. PEG-6000 was inhibited as the PCM for the investigation. Four different configurations of plate fins, which acts as enhancers of thermal conductivity, 1 plate fin, 2 plate fins, 3 plate fins and 4 plate fins for three different heat fluxes 2.0 kW/m^2 , 2.5 kW/m^2 , and 3.0 kW/m^2 . The propagation of melt front of heat sinks is investigated with the help of a digital camera. The analysis of time-temperature distribution for three values of heat flux and the operating time enhancement for different combination of fins is carried out. Results from the investigation show that due to the increased fin number, the temperature of the base of the heat sink was kept to a comparatively low value for a more extended period, than heat sinks with no fins. The highest increase in operation time is achieved with a heat flow of 3.0 kW/m^2 in the case of four finned heat sink.

Next study reports the thermal performance of various cross finned heat sinks involving PEG-6000/EG and PEG-6000/MWCNT composites for thermal management applications. The performance of various heat sink configurations namely, heat sink with one cavity (HSOC), heat sink with four cavities (HSFC), heat sink with nine cavities (HSNC), and heat sink with sixteen cavities (HSSC) are analyzed for different heat flux values ($q'' = 1.7 \text{ kW/m}^2$ to 2.4 kW/m^2). Polyethylene glycol-6000 (PEG-6000) is considered as phase change material (PCM); while expanded graphite (EG) and multi-walled carbon nanotubes (MWCNT) with varied weight concentrations (0.5, 1.0 and 2.0%) are used to prepare composite

PCM (CPCM). The characterization has been made to access various thermophysical properties and thermal stability of CPCMs. The thermal performance of heat sinks involving CPCM is estimated by analyzing the enhancement ratio and the modified Stefan Number. A maximum enhancement of 55.80% in thermal conductivity is achieved for CPCM involving PEG-6000 and 2.0% MWCNT compared to only PEG-6000. The maximum value of enhancement ratio is found to be 1.37 and 1.18 for HSFC with with PEG-6000 and 2.0 wt% EG at $q'' = 1.7 \text{ kW/m}^2$ and $q'' = 2.4 \text{ kW/m}^2$, respectively. The minimum value of modified Stefan number (St) is found to be 8.25 and 11.65 at $q'' = 1.7 \text{ kW/m}^2$ and $q'' = 2.4 \text{ kW/m}^2$, respectively for PEG-6000 and 2.0 wt% EG. The findings suggest that the HSFC with PEG-6000 and 2.0 wt% EG CPCM has the potential to enhance the thermal performance of heat sinks and can be incorporated for efficient thermal management of electronic components.

Keywords: *Phase change materials (PCM), Composite phase change materials (CPCM), PEG-6000, Plate finned heat sinks, Cross-finned heat sinks, Thermal performance.*

LIST OF PUBLICATIONS

International Journals:

- 1) **Pradunmya Pran Dutta**, Vivek Saxena, Anuj Kumar, Santosh K. Sahu, Investigation of finned heat sinks with PEG-6000/EG and PEG-6000/MWCNT composite phase change material for thermal management application. *Journal of Energy Storage* 70 (2023) 108057, (I.F. = 8.907) <https://doi.org/10.1016/j.est.2023.108057>

Book chapters:

- 1) **Pradunmya Pran Dutta**, Vivek Saxena, Santosh K. Sahu, Thermal performance analysis of phase change material-based plate finned heat sinks for thermal management applications, *Advances in Clean Energy and Sustainability, Proceedings of the ICAER 2022 conference, July 7 – 9, 2022, IIT Bombay*. https://doi.org/10.1007/978-981-99-2279-6_42
- 2) Vivek Saxena, Aastha Luthra, **Pradunmya Pran Dutta**, Santosh K. Sahu, Shailesh I. Kundalwal, Experimental investigation on phase change material enhanced pin finned heat sinks for thermal management applications, *Advances in Clean Energy and Sustainability, Proceedings of the ICAER 2022 conference, July 7 – 9, 2022, IIT Bombay*. https://doi.org/10.1007/978-981-99-2279-6_67

TABLE OF CONTENTS

1. ABSTRACT	i
2. LIST OF PUBLICATIONS	iii
3. LIST OF FIGURES	ix
4. LIST OF TABLES	xiii
5. NOMENCLATURE	xv
6. Chapter 1: Introduction	1
1.1 General background	1
1.2 Thermal energy storage (TES)	2
1.2.1 Sensible heat storage (SHS) systems	2
1.2.2 Latent heat storage (LHS) systems	3
1.2.3 Thermo-chemical reaction heat storage (TCHS) systems	3
1.3 Thermal management techniques	5
1.4 Phase change material (PCM)	5
1.4.1 Classification of phase change material	6
1.4.2 Applications of phase change material	8
1.4.3 Challenges of phase change material	8
1.5 Thermal conductivity enhancement techniques in phase change material	9
7. Chapter 2: Review of Past Work and Problem Formulation	11
2.1 Studies on PCM based heat sinks	11
2.2 Studies on PCM based heat sinks with fins	12
2.3 Studies on PCM based heat sinks with nanoparticles	16
2.4 Studies on PCM based heat sinks with expanded graphite	19
2.5 Scope of the present investigation	21
2.6 Organization of the Thesis	22

8. Chapter 3: Experimental investigations into the thermal performance of phase change material-based finned heat sinks for thermal management applications	23
3.1 General background	23
3.2 Experimental setup and methodology	24
3.2.1 Heat sinks configurations	27
3.2.2 Uncertainty and heat loss in measurement	29
3.2.3 Preparation of composite PCM (CPCM)	30
3.2.4 Experimental procedure	32
3.3 Characterization of PCM and CPCM	33
3.3.1 DSC analysis of PEG-6000	33
3.3.2 DSC analysis of PEG-6000 and composite PCM	34
3.3.3 FESEM and EDS analysis of additives and CPCM	36
3.3.4 Thermal conductivity measurement of PEG-6000 and CPCM	37
3.3.5 TGA and DTG analysis of PEG-6000 and CPCM	38
3.4 Data reduction	40
3.5 Results and discussions	41
3.5.1 Thermal performance analysis of phase change material-based plate finned heat sinks for thermal management applications	41
3.5.2 Investigation of finned heat sinks with PEG-6000/EG and PEG-6000/MWCNT composite phase change material for thermal management application	48
3.6 Concluding remarks	60
9. Chapter 4: Conclusions and Scope for Future Work	61
4.1 Thermal performance analysis of phase change material based plate finned heat sinks for thermal management applications	61
4.2 Investigating finned heat sinks with PEG-6000/EG and PEG-6000/MWCNT composite phase change material	62

for thermal management application	
4.3 Scope of future work	63
10. REFERENCES	65

LIST OF FIGURES

Fig. 1.1	Principle of sensible heat storage	2
Fig. 1.2	Application of sensible heat storage (water tank storage) [6]	2
Fig. 1.3	Principle of latent heat storage	3
Fig. 1.4	Application of latent heat storage (trombe wall) [6]	3
Fig. 1.5	Principle of thermo-chemical reaction heat storage	4
Fig. 1.6	Application of thermo-chemical reaction heat storage (boron acid-boron oxide reaction system) [7]	4
Fig. 1.7	Classification of thermal management techniques	5
Fig. 1.8	Phase change process	6
Fig. 1.9	Polyethylene glycol-6000 as phase change material	6
Fig. 1.10	Classification of PCM [10]	7
Fig. 1.11	Techniques for the enhancement of thermal conductivity of PCMs	9
Fig. 2.1	Photographic view of various heat sinks employed by Baby and Balaji [40,41]	12
Fig. 2.2	Photographic view of various heat sinks employed by Xu et al. [42]	13
Fig. 2.3	Photographic view of various heat sinks employed by Ali et al. [43]	13
Fig. 2.4	Photographic view of various heat sinks employed by Baby and Balaji [45]	14
Fig. 2.5	Photographic view of various heat sinks employed by Leong et al. [49]	15
Fig. 3.1	Illustrative representation of the experimental setup	25
Fig. 3.2	Photographic view of the experimental setup	25
Fig. 3.3	Photographic view of slots for placing the thermocouples (a) bottom of the heat sink and (b) side	26

	of the heat sink	
Fig. 3.4	Different heat sink configurations (a) HSNF, (b) HSOF, (c) HSTF, (d) HSTHF, and (e) HSFF	27
Fig. 3.5	Photographic view of various heat sinks (a) HSOC, (b) HSFC, (c) HSNC, and (d) HSSC	28
Fig. 3.6	Schematic of the fabrication method of CPCPM	32
Fig. 3.7	Differential Scanning Calorimetry heating of PEG-6000	33
Fig. 3.8	DSC curves comparing PEG-6000 and various CPCPMs during (a) heating and (b) cooling	34
Fig. 3.9	FESEM and EDS analysis of (a) EG, (b) MWCNT, (c) PEG-6000/EG-CPCPM (0.5 wt%), and (d) PEG-6000/MWCNT-CPCPM (0.5 wt%)	36,37
Fig. 3.10	Thermal conductivity enhancement of CPCPM	38
Fig. 3.11	TGA and DTG analysis of (a) PEG-6000 (b) PE1 (c) PE2 (d) PE3 (e) PM1 (f) PM2, and (g) PM3	39,40
Fig. 3.12	Temperature variation with time for HSNF (a) without PCM, and (b) with PCM	42
Fig. 3.13	Temperature variation with time for various heat sink layouts at various heat fluxes (a) 2.0 kW/m ² , (b) 2.5 kW/m ² , and (c) 3.0 kW/m ²	43
Fig. 3.14	Propagation of melt front for (a) HSNF, (b) HSOF, (c) HSTF, (d) HSTHF, and (e) HSFF	45,46
Fig. 3.15	Time needed to reach critical ST by various layouts of heat sinks for different values of heat flux (a) 65°C and (b) 70°C	47
Fig. 3.16	Enhancement ratio for various layouts of heat sink with different values of heat flux at ST of (a) 65°C and (b) 70°C	47
Fig. 3.17	Comparison of present experimental results with the results of other researchers for (a) Heat sink without	49

	PCM and (b) Heat sink with PCM	
Fig. 3.18	Temperature variation with time for an unfinned heat sink for (a) $q'' = 1.7 \text{ kW/m}^2$ and (b) $q'' = 2.4 \text{ kW/m}^2$	50
Fig. 3.19	Time to attain the temperature of $85 \text{ }^\circ\text{C}$ for heat sink with (a) PEG-6000, (b) PE1, and (c) PM1 for HSOC	51
Fig. 3.20	Temperature variation with time to reach a temperature of $85 \text{ }^\circ\text{C}$ at $q''=1.7 \text{ kW/m}^2$ for (a) HSOC, (b) HSFC, (c) HSNC, and (d) HSSC	52
Fig. 3.21	Temperature variation with time to reach a temperature of $85 \text{ }^\circ\text{C}$ at $q''=2.4 \text{ kW/m}^2$ for (a) HSOC, (b) HSFC, (c) HSNC, and (d) HSSC	53
Fig. 3.22	Temperature variation with time to reach a temperature of $85 \text{ }^\circ\text{C}$ at $q''=1.7 \text{ kW/m}^2$ for (a) PEG-6000, (b) PE1, (c) PE2, (d) PE3, (e) PM1, (f) PM2, and (g) PM3	54,55
Fig. 3.23	Temperature variation with time to reach a temperature of $85 \text{ }^\circ\text{C}$ at $q''=2.4 \text{ kW/m}^2$ for (a) PEG-6000, (b) PE1, (c) PE2, (d) PE3, (e) PM1, (f) PM2, and (g) PM3	56,57
Fig. 3.24	Comparison of modified Stefan number with time to reach a temperature of $85 \text{ }^\circ\text{C}$ for (a) PEG-6000, (b) PE1, (c) PE2, (d) PE3, (e) PM1, (f) PM2, and (g) PM3	58,59
Fig. 3.25	Enhancement ratio at a heat flux of (a) 1.7 kW/m^2 , and (b) 2.4 kW/m^2 for a ST of $85 \text{ }^\circ\text{C}$	60

LIST OF TABLES

Table 1.1	Studies on applications of PCM	8
Table 3.1	Thermophysical properties of various materials [95]	26
Table 3.2	Fin dimensions of the heat sinks in use [96]	28
Table 3.3	Dimensions of the cross-finned heat sinks [50]	29
Table 3.4	Geometrical specifications and characteristics of expanded graphite (EG) and multi-walled carbon nano-tubes (MWCNT)	31
Table 3.5	Thermal energy storage properties of PEG-6000, PEG-6000/EG, and PEG-6000/MWCNT composite PCMs	35

NOMENCLATURE

Symbols

A	Area of heat sink (m^2)
C	Specific heat capacity (kJ/kg.K)
e	Thermal effusivity ($\text{kJ/m}^2.\text{K.s}^{1/2}$)
Er	Enhancement ratio
k	Thermal conductivity (W/m.K)
l	Length of the HS (mm)
L	Latent heat (kJ/kg)
q''	Heat flux (kW/m^2)
Q	Total heat energy (kW)
St	Modified Stefan Number
T	Temperature ($^{\circ}\text{C}$)
wt	Weight (mg)

Greek symbols

φ	Additive mass fraction
ρ	Density (kg/m^3)

Abbreviations

ATMS	Active thermal management system
CPCM	Composite phase change material
DSC	Differential scanning calorimetry
DTG	Derivative thermogravimetry
EDS	Energy dispersive X-ray spectroscopy
EG	Expanded graphite
EHS	Empty heat sink
EPCM	Encapsulated phase change material
FESEM	Field emission scanning electron microscopy
HS	Heat sink
HSNF	Heat sink with no fin
HSOF	Heat sink with one fin

HSTF	Heat sink with two fin
HSTHF	Heat sink with three fin
HSFF	Heat sink with four fin
HSOC	Heat sink with one cavity
HSFC	Heat sink with four cavities
HSNC	Heat sink with nine cavities
HSSC	Heat sink with sixteen cavities
HTF	High temperature fluid
HTMS	Hybrid thermal management system
LHS	Latent heat storage
MPCM	Micro-encapsulated phase change material
MWCNT	Multi-walled carbon nanotubes
NePCM	Nano-enhanced phase change material
PCM	Phase change material
PEG-6000	Polyethylene glycol-6000
PE1	EG dispersed PCM (0.5 mass%)
PE2	EG dispersed PCM (1.0 mass%)
PE3	EG dispersed PCM (2.0 mass%)
PFHS	Pin fin heat sink
PM1	MWCNT dispersed PCM (0.5 mass%)
PM2	MWCNT dispersed PCM (1.0 mass%)
PM3	MWCNT dispersed PCM (2.0 mass%)
PTMS	Passive thermal management system
SHS	Sensible heat storage
ST	Set-point temperature
TCE	Thermal conductivity enhancer
TCHS	Thermo-chemical reaction heat storage
TES	Thermal energy storage
TGA	Thermogravimetric analysis
TM	Thermal management

Chapter 1

Introduction

1.1 General background

The advancement in technology and compact size of modern electronics components increases the power density of electronic components. These components generate substantial amount of heat that leads to decrease in the thermal performance and reduces the operating life [1,2]. The thermal management (TM) of these electronic components has become a critical concern for researchers during the design and manufacturing processes. In such a case, it is crucial to design and develop an advanced and reliable cooling module that can dissipate the excess heat and maintain the components at safe operating temperature. Excessive rise in temperatures is a major cause of electronics failure; with 1% decrease in temperature can reduce the failure rate by 4%, while with 10-20 °C increase in temperature may lead to a 100% increase in failure rate [3]. It is argued that 50% of electronic device failures occurs due to temperature-related issues [4]. Therefore, it is essential to maintain safe temperature limits, safe and reliable operation of electrical devices.

In view of this, various cooling techniques have been employed to cool electronic chips in recent years; these include active cooling and passive cooling. Active cooling methods usually incorporate external equipment such as fans or pumps, that increase installation and maintenance costs [5], therefore, active cooling techniques are less frequently employed for cooling modules. This necessitates the adoption of reliable, efficient, and passive cooling techniques for thermal management applications. These are usually employed in heat sinks for thermal management of electronic components.

1.2 Thermal energy storage (TES)

Thermal energy storage (TES) is a technique that involves storing thermal energy through the process of heating or cooling a material. This allows the energy to be preserved and utilized in the future for various applications, such as heating and cooling systems, as well as power generation. TES not only reduces the discrepancy between the demand and supply by conserving energy, but also improves the performance and thermal reliability of the system. The methods of TES systems are elaborated here:

- Sensible heat storage systems
- Latent heat storage systems
- Thermo-chemical reaction storage systems

1.2.1 Sensible heat storage (SHS) systems

Sensible heat storage (SHS) is the process of storing thermal energy by raising the temperature of a solid or liquid. The amount of heat stored depends on a number of variables, including the specific heat capacity, the degree of temperature change, and the mass of storage material used. Fig. 1.1 shows the principle of sensible heat storage in SHS material while Fig. 1.2 depicts the application of sensible heat storage in controlling the water temperature.

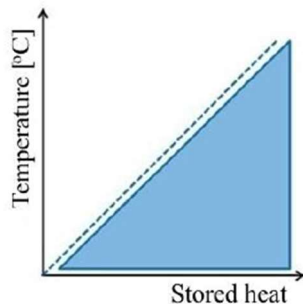


Fig. 1.1 Principle of sensible heat storage

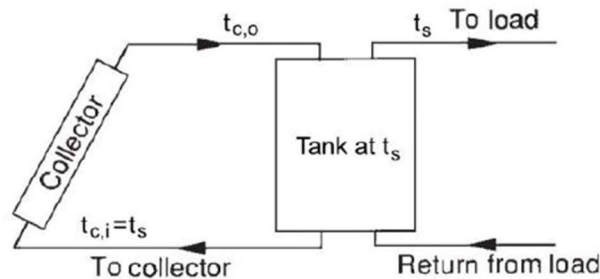


Fig. 1.2 Application of sensible heat storage (water tank storage) [6]

1.2.2 Latent heat storage (LHS) systems

Latent heat thermal energy storage (TES) is a type of energy storage system that utilizes the latent heat of a phase change material (PCM) to store and release thermal energy. In latent heat TES, energy is stored and released by changing the phase of the PCM, typically from solid to liquid or liquid to gas, and vice versa. The amount of heat stored depends on a number of variables, including the specific heat capacity, the degree of temperature change, and the mass of storage material used. Fig. 1.3 shows the principle of heat storage in LHS material, while Fig. 1.4 depicts the application of LHS material in a trombe wall.

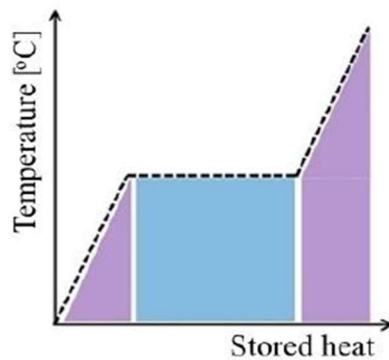


Fig. 1.3 Principle of latent heat storage

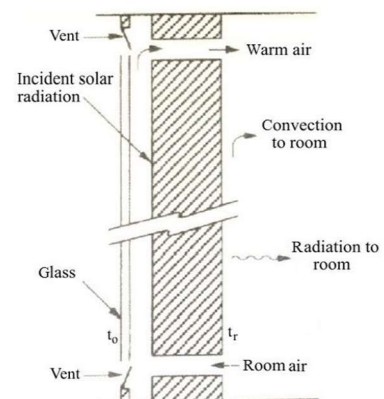


Fig. 1.4 Application of latent heat storage (trombe wall) [6]

1.2.3 Thermo-chemical reaction heat storage (TCHS) systems

Thermochemical systems utilize reversible chemical reactions that involve the breaking and formation of molecular bonds to absorb and release energy. The amount of heat stored in these systems depends on various factors such as the quantity of storage material, the endothermic heat of the reaction, and the extent conversion. Fig. 1.5 shows the principle of thermo-chemical reaction heat storage of heat in TCHS

material, while Fig. 1.6 shows the application of thermo-chemical reaction heat storage.

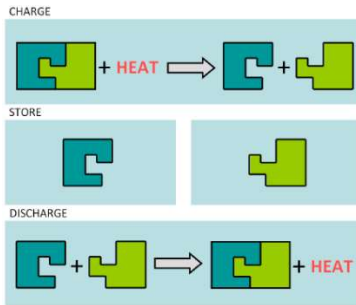


Fig. 1.5 Principle of thermo-chemical reaction heat storage

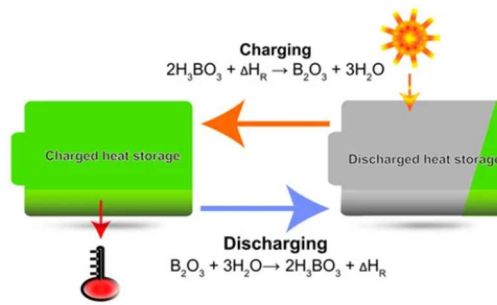


Fig. 1.6 Application of thermo-chemical reaction heat storage (boron acid-boron oxide reaction system) [7]

Among various TES systems, latent heat based TES system is found to be superior compared to other systems. The advantages of latent heat based TES are elaborated below:

- Latent heat storage systems have a higher energy storage density compared to thermo-chemical and sensible heat storage. This allows for efficient energy storage in a smaller volume or mass of material.
- Latent heat storage systems maintain a nearly constant temperature during the phase change process.
- The high energy storage density of latent heat storage allows for more compact system designs compared to thermochemical and sensible heat storage systems.
- Latent heat storage materials generally exhibit good thermal stability during repeated phase change cycles. They can withstand numerous heating and cooling cycles without significant degradation, ensuring the long-term performance and reliability of the system.

1.3 Thermal management techniques

Thermal management techniques refer to numerous methods used to control and regulate the temperature of systems, or components. Thermal management techniques are mainly of three types: active thermal management system (ATMS), passive thermal management system (PTMS), and hybrid thermal management system (HTMS).

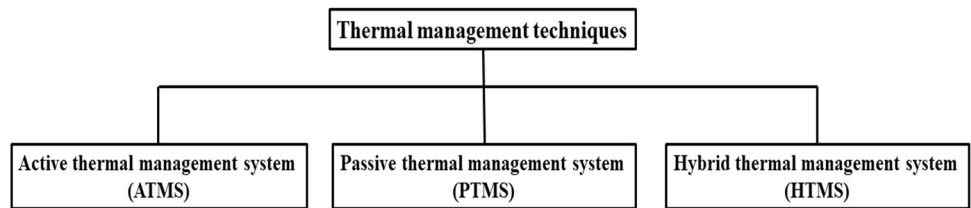


Fig. 1.7 Classification of thermal management techniques

ATMS cooling methods usually rely on an external power supply. This approach achieves the desired cooling by increasing the flow rate of a heat transfer fluid. It involves actively circulating different fluids such as air and water. Additionally, thermoelectric coolers can be employed for cooling purposes. PTMS can be defined as a set of cooling methods that operate without the need for an external power source. These techniques aim to dissipate heat generated by the devices through natural conduction, convection, and radiation processes, without actively circulating a heat transfer fluid. Passive thermal management techniques usually rely on the design and selection of materials with high thermal conductivity and efficient heat dissipation properties. HTMS can be defined as a combination of active and passive cooling methods employed to effectively manage the heat generated by various thermal systems.

1.4 Phase Change Material (PCM)

PCMs are latent heat storage materials that can store and release large amounts of thermal energy during the process of phase transition, such as melting or solidification. PCM utilizes latent heat to store the

energy during the phase transition process. However, due to high volume changes and high pressure, the phase transition in PCM during thermal management application is limited to solid-liquid phase change [8]. PCMs absorb and release heat at a nearly constant temperature; these materials 5–14 times more heat per unit volume than sensible storage materials [9].

Fig 1.8 illustrates the solid-liquid phase change process in an ideal PCM based thermal management system. Initially, the phase change material exists in a solid state at a certain temperature below its melting point. When the heat is applied to the solid PCM, its temperature begins to rise and heat energy is absorbed by the material. This process continues until the temperature reaches the melting point of the material. At the melting point, PCM undergoes a phase transition from a solid to a liquid state. During this transition, the material absorbs a significant amount of heat energy from the surroundings, known as the latent heat of fusion. This whole process can be termed as charging process. During the discharging process, the order of the process gets reversed.

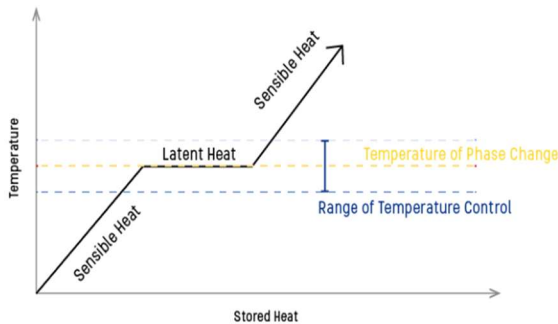


Fig. 1.8 Phase change process



Fig. 1.9 Polyethylene glycol - 6000 as phase change material

1.4.1 Classification of phase change material

Phase change materials (PCMs) can be classified based on their chemical composition. Fig 1.10 illustrates the classification of PCM based

on their chemical composition. The classification of PCM are detailed below:

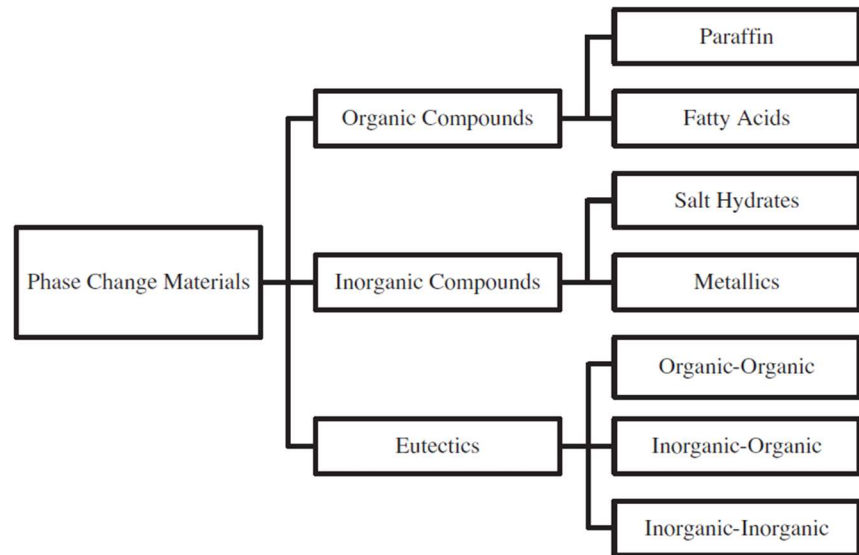


Fig. 1.10 Classification of PCM [10]

1. Organic PCMs: Organic PCMs are composed of carbon-based compounds and are known for their relatively low melting points and good thermal stability. The thermophysical characteristics of organic PCMs include the latent heat values ranging from 100-310 J/g, thermal conductivity between 0.14 and 0.4 W/m.K, specific heat ranging from 1.5-2.9 J/kg.K, and density varying within the range of 0.7-1.4 kg/m³ [11–14].
2. Inorganic PCMs: Inorganic PCMs are composed of inorganic compounds, including salts and metallic alloys. They have higher melting points compared to organic PCMs and can store larger amounts of thermal energy. The thermophysical characteristics of inorganic PCMs include the latent heat values ranging from 90-495 J/g, thermal conductivity between 0.5 and 1.3 W/m.K, specific heat ranging from 2.5-5 J/kg.K, and density varying within the range of 1.3-2.5 kg/m³ [11–14].

3. Eutectic PCMs: Eutectic PCMs are a specific category of phase change materials that consist of a mixture of different substances with unique composition. Eutectic PCMs include both organic and inorganic compounds. They are designed to have a specific melting point and are commonly used for precise temperature control applications.

1.4.2 Applications of phase change material

Phase change materials (PCMs) have a wide range of applications that include thermal energy storage, electronics cooling, temperature regulation in transportation, and waste heat recovery. Table 1.1 presents studies by various researchers on applications of PCM.

Table 1.1 Studies on applications of PCM.

Applications	References
Thermal management of electronic components	Sahoo et al. [15], Cai et al. [16]
Thermal energy storage	Abokersh et al. [17], Khan et al.[18], Xu et al. [19]
Waste Heat Recovery	Gutierrez et al. [20], Nomura et al. [21], Shon et al. [22]
Thermal management of battery modules	Kim et al. [23], Siddique et al. [24]
Thermal management of PV panels	Islam et al. [25], Waqas et al. [26]
Satellite thermal management	Raj et al. [27], Kansara et al. [28]

1.4.3 Challenges of phase change material

While phase change materials (PCMs) offer numerous benefits, they also have some challenges that need to be considered. These challenges include low thermal conductivity, volume expansion during

phase change, supercooling and superheating, cost of PCM, degradation, and compatibility with other materials.

It is important to note that the disadvantages of PCMs can vary depending on the specific material, application, and operating conditions. These drawbacks should be carefully considered along with the advantages while evaluating the suitability of PCMs for the specific application. However, it is observed that organic PCMs exhibit superior thermal stability, non-toxicity, non-corrosiveness, and minimal or no subcooling. Organic PCMs offer a wide temperature range, making them suitable for applications in thermal management and thermal energy storage. Most of the organic PCMs possess lower value of thermal conductivity [29]. In order to improve the low thermal conductivity, thermal conductivity enhancers (TCEs) such as metallic fins, additives such as nanoparticles and microparticles (expanded graphite), metal foam (porous matrix), and encapsulation are employed in PCM.

1.5 Thermal conductivity enhancement techniques in PCM

The low thermal conductivity of PCM results in lower heat transfer rate and lower heat storage/release rate, which is a major drawback for their practical applications. With the enhancement in the thermal conductivity of PCMs, the heat storage, and release rate can be improved which can enhance the efficiency of the system. Fig 1.7 represents the various techniques which help in increasing the thermal conductivity of PCMs.

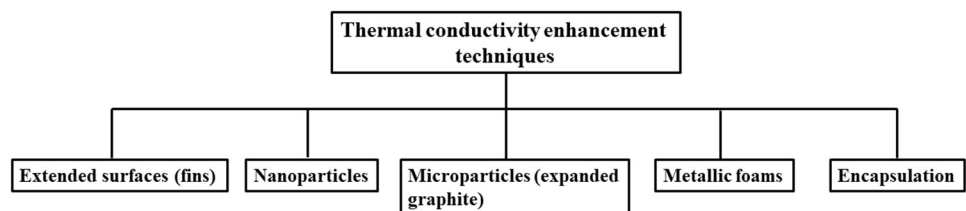


Fig. 1.11 Techniques for enhancement of thermal conductivity of PCMs.

The following sub-section provides an elaboration on the different techniques employed to enhance thermal conductivity in phase change materials.

1. Extended surfaces: Incorporating fin configurations with PCM can expedite both melting and solidification processes. This concept was first proposed by Abhat et al. [11] and subsequently implemented by Humphrey et al. [30].
2. Addition of nanoparticles: The addition of nanoparticles to phase change materials (PCMs) offers several advantages and can lead to enhanced performance [31,32]. Nanoparticles have a high surface-to-volume ratio due to their small size, which significantly increases the contact area between the PCM and the nanoparticles. This increased surface area promotes efficient heat transfer and enhances the overall thermal performance of the PCM.
3. Microparticles (expanded graphite): The most regular form of graphite is flake graphite, which shows great thermal properties with high thermal conductivity. Expanded graphite (EG) is made by natural flake graphite exhibits superior thermal conductivity due to its layered structure, lower density, chemical stability, and high aspect ratio [33].
4. Metallic foams: Metallic foams have a highly porous structure with interconnected pores. This structure provides increased surface area and improves the contact with PCM.
5. Encapsulation: The encapsulated phase change material (EPCM) is made up of core and shell by emulsion polymerization, interfacial polymerization, and mini-emulsion polymerization. The PCM and the polymer (or inorganic material) is utilized as core and shell, respectively. The EPCM has a remarkable ability to enhance thermal conductivity of PCM [34]. It also restricts the direct contact of PCM with the environment. During the phase change, microencapsulated PCM provides controllable volume [35].

Chapter 2

Review of Past Work and Problem Formulation

Various studies have been made to enhance the thermal performance of PCM-based heat sinks. These include the selection of PCM for latent heat thermal energy storage and PCM-based passive cooling. Also, efforts have been made to analyse the effect of different TCEs such as fins, and metallic/non-metallic microparticles and nanoparticles to augment the performance of PCM-based heat sinks. The studies relevant to the present dissertation are reported in the subsequent sections.

2.1 Studies on PCM based heat sinks

Hassab et al. [36] conducted a numerical study that introduces a computational model to analyze the melting of wax within a vertical cylinder. Two models were employed; the first model (Approach-I) utilized a constant value for the density of the phase change material (PCM), while the second model (Approach-II) incorporated a variable density. Zivkovic and Fujii [37] conducted a numerical investigation to analyze the phase change process of phase PCM in rectangular and cylindrical containers. They simulated the dynamic behavior of PCM confined within a container and reported that the conduction heat transfer within the PCM along the direction of the high temperature fluid (HTF) is insignificant. Ismail and Jesus [38] conducted a parametric investigation on the solidification process of phase change material (PCM) around a cylinder for ice-bank applications. Tan et al. [39] conducted a computational study to analyze the influence of buoyancy-driven convection during the confined melting of PCM within a spherical capsule. The findings indicate significant thermal stratification of the

molten liquid in the upper half of the sphere; this is attributed to the upward movement of the molten liquid along the inner surface of the sphere, which displaces the colder fluid.

2.2 Studies on PCM based heat sinks with fins

Extended surfaces, also known as fins, are often incorporated into PCM-based heat sinks to enhance their thermal performance. Various studies have been conducted employing fins in PCM based heat sinks. Baby and Balaji [40] conducted experiments to analyse the performance of PCM based heat sinks for cooling of portable electronics. The dimensions of the heat sink used in the study is $80 \times 62 \times 25 \text{ mm}^3$ with the power level varying between 2 to 7 W. They considered n-eicosane as PCM and heat sinks involve plate fins made of aluminum. They reported that a pin fin heat sink provides an enhancement factor of 18 compared to the heat sink without fins, when tested at a $45 \text{ }^\circ\text{C}$ SPT and 7 W of power. In another study [41], the authors reported the use of a 7 plate-fin heat sink that can result an enhancement factor of 15 in the operating time compared to the heat sink without fins (used as a baseline for comparison). Figure 2.1 reports the photographic view of various heat sinks employed by Baby and Balaji [40,41].



Fig 2.1 Photographic view of various heat sinks employed by Baby and Balaji [40,41]

In a study made by Xu et al. [42], the authors employed n-docosane as PCM under hypergravity of 0-6 g. For pin fin heat sink (PFHS), the maximum variation in the total melting time between hypergravity, and normal gravity conditions is found to be 15.9%. While

considering the high heat flux conditions, the inclusion of pin fins results in a reduction in the complete melting time for hypergravity conditions. Figure 2.2 represents two different heat sinks EHS and PFHS used by the authors. Ali et al. [43] conducted experimental investigations using six PCMs SP-31, RT-35HC, RT-44, RT-54, n-eicosane, and paraffin wax for rectangular, triangular, and pin-finned heat sinks. The power levels are between 5 to 8 W. During the analysis of storage ratio, it was observed that RT-35HC had the highest storage ratio of 68 % and 38.5 % at 5 W and 8 W, respectively, while SP-31 exhibits the second highest storage ratio of 63% and 36% at 5 W and 8 W, respectively. The SP-31 exhibits the highest enhancement ratio for PCM at a set-point temperature (ST) of 45 °C. On the other hand, for a critical ST of 60 °C, RT-54 was found to be the best option. Figure 2.3 shows different heat sinks that employ pin fins with different cross-sections.

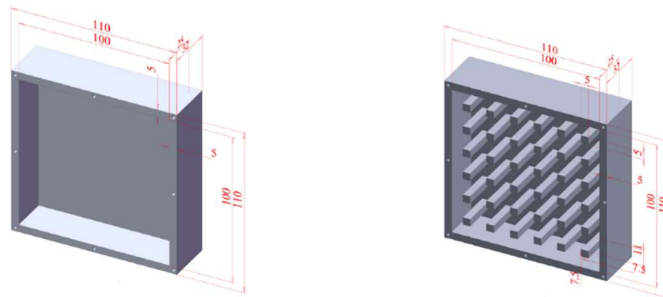


Fig 2.2 Photographic view of various heat sinks employed by Xu et al. [42]

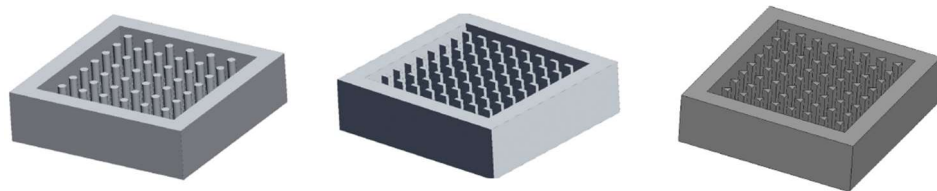


Fig 2.3 Photographic view of various heat sinks employed by Ali et al. [43]

Kim et al. [44] used paraffin as PCM and investigated the thermal efficiency of heat sinks with PCM for cooling high-power electronics. The thermal resistance of the PCM-integrated fin-type heat sinks is comparable to that of conventional fin-type heat sinks. Baby and Balaji [45] conducted experimental investigations using n-eicosane as PCM under constant and intermittent loads, with power levels of 5 to 10 W. The analysis shows that when the total heat input is kept constant (48 kJ) and the operation duration is fixed (160 min), the peak temperature of the heat sink side wall reduces by 11.9 °C. Figure 2.4 show the heat sink used by the authors in their investigation.

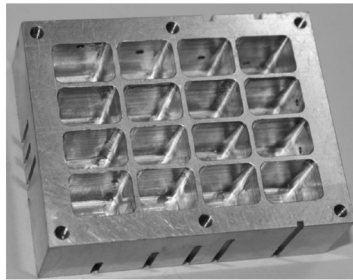


Fig 2.4 Photographic view of various heat sinks employed by Baby and Balaji [45]

In their studies, Arshad et al. [46,47] investigated the impact of various factors, such as pin fin types (square, round), number of fins, heat flux values (ranging from 1.58 to 3.2 kW/m²), PCM volume fraction, and different heat sink configurations, on the thermal performance. With the PCM volume fraction of 1, the heat sinks with round pin fins having a diameter of 3 mm and heat sinks with square pin fins with a thickness of 2 mm enhance the operating time to attain the set-point temperature. The highest enhancement ratios in operating time is found to be 4.2 and 4.3 for round pin fins and square pin fins, respectively. Mahmoud et al. [48] conducted experimental investigations on honeycomb matrix-based heat sinks with cross and parallel fins, using six different PCMs. Their findings indicated that the honeycomb structure offers superior performance as

compared to finned heat sinks. Through experimental investigation, Leong et al. [49] analyzed the thermal performance of various cross fin heat sink configurations, heat sink with no fin, heat sink with 9 square cross fins and 16 square cross fins, filled with different PCM volume fractions. The study utilized 1-hexadecanol and paraffin wax as PCM materials. Among various configurations, the heat sink incorporating 16 square cross fins with paraffin wax demonstrated superior heat transfer performance compared to the other configurations using 1-hexadecanol. Figure 2.4 show the heat sink in used in their investigation. Kumar et al. [50] experimentally investigated cross-finned heat sinks employing paraffin wax as the PCM. The heat sink with 36 cavities attains a maximum enhancement ratio of 6.5 when the heat flux is 1.5 kW/m^2 and the set-point temperature (ST) is 65°C . However, as the heat flux and ST value increases, the enhancement ratio gradually decreases and reported that forced convection should be used to achieve faster cooling rate.



Fig 2.5 Photographic view of various heat sinks employed by Leong et al. [49]

In their numerical study, Pourhemmati and Hossainpour [51] proposed a vertical plate-fin heat sink (PFHS) with variable fin thickness to address thermal issues under natural convection. The thermal performance of the variable fin PFHS is highly influenced by the fin convergence angle, particularly when the fin density is high. Nayak et al. [52] proposed a numerical model for PCM based heat sinks and TCEs. The study investigates two thermal conducting elements (TCEs) such as PCM within a porous TCE matrix and PCM with TCE fins. The results indicate that thinner fins perform better compared to other fins and also

found that rod-type fins outperform plate-type fins. In the numerical analysis, Jeon and Byon [53] investigated the horizontal PFHS with two dual-height fins. The fin configuration is found to reduce the specific thermal resistance, which is calculated as the product of thermal resistance and heat sink weight. Zhang et al. [54] presented a novel W-type fin design for a vertical heat sink for different values of inclined angle, fin spacing, fin height, and gap clearance. The proposed designs exhibit more uniform temperature distribution compared to conventional plate-fin heat sinks. Abbas and Wang [55] conducted both experimental and numerical analyses of a vertical plate-fin heat sink (PFHS); significant reduction in the thermal resistance is obtained for PFHS. Akula et al. [56] investigated a heat sink based on PCM with various orientations through both numerical and experimental investigations. The horizontal orientation of heat sink exhibits the best performance with respect to the discharging time. A vertical heat sink design with a variable height fin array was presented by Huang et al. [57]. For the variable height heat sink, optimisation studies were carried out to reduce thermal resistance and material cost per power unit.

2.3 Studies on PCM based heat sinks with nanoparticles

PCM based heat sinks with nanoparticles refer to the integration of nanoparticles, with dimensions ranging from 1 to 100 nm, in the PCM. Numerous studies have been made to analyze the thermal performance of nanoparticle enhanced PCM based heat sinks. Arshad et al. [58] made a novel composite comprising of RT-28HC as PCM and MWCNTs, graphene nanoplatelets (GNPs), aluminium oxide (Al_2O_3), and copper oxide (CuO) as nanoparticles. The findings of the study states that in comparison of mono and hybrid nano-enhanced PCMs (NePCMs), the results exhibit the performance of hybrid NePCM with GNPs/MWCNTs at mass percentage ratio of 75%/25% had the highest thermal conductivity enhancement of 96% compared to the pure PCM. The hybrid NePCM of

RT-28HC/GNPs+MWCNTs exhibit more uniform heating over an extended melting duration compared to RT-28HC/Al₂O₃+CuO and pure RT-28HC. Zhang et al. [59] reported that the use of polyethylene glycol (PEG) as a PCM, to prevent the leakage issues during phase transition. A ternary eutectic phase change material (PCM) consisting of oleic acid, isopropyl palmitate, and butyl stearate with mole fractions of 0.44, 0.33, and 0.23 is developed by Dinesh et al. [60]. The authors used the nanoparticles (MWCNT) in various mass percentages (0.02, 0.04, 0.06, 0.08 and 0.10), to examine the thermal behavior of the NePCM. The heat transfer rate during the solidification process is found to enhance by 34.45% for 0.10 mass percentage of MWCNT. There is a slight decrease in the phase change temperature and latent heat storage capacity. Additionally, the prepared ternary eutectic PCM with 0.10 mass percentage of MWCNT exhibits heat loss efficiencies of 0.13% (before thermal cycle) and 0.12% (after thermal cycle). The ternary eutectic PCM possesses thermal reliability even after undergoing 500 thermal cycles. The thermophysical attributes of a binary eutectic PCM consisting of LiNO₃, MWCNT nanoparticles and NaCl are examined by Kumar et al. [61]. Experimental analysis of the charging and discharging characteristics of NePCM confirms that the addition of nanoparticles reduce the charging and discharging times. Murugan et al. [62] examined the thermophysical properties of the NePCM using MWCNT as an additive. The addition of 0.3 wt.% MWCNTs to the NePCM results in a maximum reduction of 30% in melting time compared to the base PCM. Ali [63] recommended the use of nanoparticle-enhanced RT-35HC for low heat flux applications with heat flux ranging between 1.0 to 2.5 kW/m². Yadav and Sahoo [64] examined the effect of natural convection on the thermal energy storage system using capric acid (CA) as PCM and MWCNT. The inclusion of 0.02% vol. fraction of MWCNT in the CA PCM results in a 66.67% reduction in melting time compared to the base CA PCM. Kumar et al. [65] reported that 0.5% mass fraction of CuO in the paraffin wax exhibits

the best performance. The maximum reduction in latent heat of fusion is found to be 24.75% at $\phi=3.0$. While the maximum enhancements in thermal conductivity and viscosity are found to be 150% and 100% respectively. For the heat sink with six pin fins (HSSPF), with pure PCM and NePCM (at $\phi=0.5$), the maximum temperature reduction is found to be 13°C and 15°C, respectively. Alimohammadi et al. [66] conducted experimental investigations on various heat sink configurations, including heat sinks without PCM, heat sinks with PCM, and heat sinks with NePCM, under both forced and free convection conditions. The authors employed $Mn(NO_3)_2$ as the PCM and Fe_3O_4 as the nanoparticles. Tariq et al. [67] considered various mass fractions (0.002, 0.005 and 0.008%) of graphite nanoparticles (GNPs) with RT-44HC and RT-64HC for the thermal management of electronic devices. Krishna et al. [68] analysed water, tricosane (pure PCM) and Al_2O_3 impregnated with tricosane (NePCM) in the heat pipe for electronic cooling applications. The NePCM-based heat pipe is found to save 53% of fan power compared to the conventional heat pipe. Arshad et al. [69] carried out a numerical analysis, in order to analyze the melting behaviour and heat transfer capabilities of a heat sink using nano-enhanced phase change material (NePCM). They added copper nanoparticles for varied range of volume fractions (0.00, 0.01, 0.03, and 0.05) to RT-28HC. The NePCM based heat sink exhibits better performance. Bondareva et al. [70] examined heat and mass transfer in a finned heat sink NePCMs; n-octadecane is used as PCM. The heat transfer efficiency is enhanced by increasing the length of the radiator fins when utilizing NePCM. Mahdi and Nsofor [71] numerically investigated the effects of adding alumina nanoparticles on the solidification process of PCM in a triplex-tube TES system. Hosseinizadeh et al. [72] investigate the unconstrained melting behaviour of a nano-enhanced phase change material (NePCM) inside a spherical container. The NePCM is made up of copper nanoparticles and RT-27 as PCM. The simulation findings show that the NePCM thermal conductivity

increases when nanoparticles are added compared to normal PCM. Kashani et al. [73] used RT-35 and silicon carbide (SiC) as PCM and nanoparticles, respectively, and found that increasing the volume fraction of nanoparticles and reducing the wall temperature leads to the increase in the solid fraction of the material. Elbahjaoui et al. [74] investigated solidification of rectangular NePCM slabs, made of n-octadecane and copper as PCM and nanoparticles, respectively; they argued that the solidification rate improved due to the presence of nanoparticles. Sushobhan and Kar [75] conducted a numerical study and observed that the thermal conductivity of n-octadecane increases with the addition of CuO nanoparticles, leading to an enhanced melting rate. Simulations of the melting of a paraffin-based nanofluid containing copper nanoparticles were performed by Sebti et al. [31]. They noticed that the rate of heat transfer is accelerated when the volume percentage of nanoparticles is increased. Faraji et al. [76] analysed the melting of NePCM in inclined rectangular enclosure. The concentration of nanoparticles in PCM is found to affect the heat transfer performance.

2.4 Studies on PCM based heat sinks with expanded graphite

Expanded graphite (EG) is usually incorporated into phase change materials (PCM) to enhance their thermal properties, and to improve stability of PCM composites. Numerous investigations have been conducted that report inclusion of EG as an TCE in PCMs. Wu et al. [77] experimentally studied PCM composite involving expanded graphite and modified aluminium potassium sulphate dodecahydrate (MAPSD) for solar energy storage. These composites are reported to be suitable for various applications such as industrial waste heat energy recovery, solar domestic hot water systems, and mid-temperature thermal energy storage systems. Wu et al. [78] investigated the thermal characteristics of the PCM composite involving EG/paraffin in a water heating system. Ren et al. [79] investigated microencapsulated PCM composite involving PCM and EG

in a cascaded pin fin heat sink. Their findings demonstrate the pin finned configuration without nanoparticles is more advantageous in low temperature conditions, while the addition of EG is advantageous at high temperature. Lin et al. [80] carried out an experimental investigation to analyze the thermal energy storage performance and phase change behavior of a latent heat energy storage system integrated with a double-spiral coiled heat exchanger. Sebacic acid (SA), which has a melting point of approximately 130 °C, is utilized as PCM and EG is used to absorb SA to prepare the form stable SA/EG composite. Huang et al. [81] prepared a composite PCM constituting of LiNO₃/KCl/EG. The inclusion of EG in the PCM (eutectic LiNO₃/KCl) does not alter the phase change temperature significantly, while it reduces the latent heat. Lv et al. [82] prepared composite PCM involving polyethylene glycol (PEG) and EG with a different mass fraction. The thermal conductivity of PCM composite improves with the addition of EG. Ma et al. [83] experimentally studied PCM composite involving paraffin wax and EG for a personal cooling system. Cai et al. [84] prepared the PCM composite involving paraffin, expanded graphite (EG), and ethylene–vinyl acetate (EVA). Akula and Balaji [85] presented a novel fin–PCM–EG composite for better thermal management of a Panasonic NCR18650BD battery. Fins and EG are augmented with PCM to enhance its effective thermal conductivity. Eicosane is used as PCM with an addition of 0, 10, 20, 25, and 30% weight fractions of EG in the heat sinks. Zhang et al. [86] prepared PCM composite involving paraffin and EG and is used for latent heat storage system. The thermal energy storage charging duration for the composite PCM is reduced compared to paraffin. Cai et al. [87] prepared a series of paraffin/expanded graphite (EG) composites with various mass fraction and proposed a numerical model to predict the effective thermal conductivity of composite PCM (CPCM).

2.5 Scope of the present investigation

It is evident that numerous studies have been made to analyze the thermal performance of PCM based heat sinks for thermal management applications. Several methods have been developed to enhance the thermal conductivity of PCM-based heat sinks for thermal management applications, including the incorporation of fins, nanoparticles, and expanded graphite. The impact of various factors on the heat transfer rate, such as heat flux values, heat sink designs, types of thermal conductivity enhancers (TCEs), and set-point temperature (ST), has been studied. However, there are still several challenges that need to be addressed regarding the implementation of PCM-based heat sinks for thermal management. These issues are outlined as follows:

- It is observed that paraffin wax is used as PCM for energy storage and thermal management applications; while, its application is limited because of various limitations such as poor chemical stability, leakage tendency, low viscosity, and super-cooling problems [88]. On the contrary, the PEG-6000 can be used as PCM as it exhibits good thermal stability, reliability, chemical stability, and small volume change during phase transition compared to paraffin wax [89].
- Most of the studies focus on numerical investigations of heat sinks employing a parallel plate-fin arrangement. It should be noted that different fin arrangements can be employed to enhance the heat transfer properties of the system. The experimental investigation of a cross plate-fin arrangement with various cavities integrated with PEG-6000 as the PCM has not been extensively examined.
- Developing composite PCMs involving PEG-6000, expanded graphite (EG), and multi-walled carbon nanotubes (MWCNT) and analyzing its thermal performance for thermal management application.

- Limited studies are available that report suitable preparation methodology , development of CPCM for different concentration of additives and characterization of CPCM to assess its thermophysical properties.

2.6 Organization of the Thesis

The present study is aimed to address some of the issues highlighted above. The aim of the present thesis is to analyse the thermal performance of PEG-6000 based heat sinks (plate finned and cross finned). Also, efforts have been made to analyse the heat transfer performance incorporating carbon-based additives like EG and MWCNT with PCM in heat sinks involving constant heat flux. Effect of various parameters such as heat sink configuration, heat flux, operating time to reach a certain set-point temperature, and additive concentration on the thermal performance is investigated experimentally. The organization of the dissertation is as follows:

Chapter 1: This chapter introduces the need for thermal management of electronic components and different cooling techniques. The chapter also introduces phase change material, applications, and challenges.

Chapter 2: The second chapter discusses the review of relevant literature pertaining to thermal management techniques and outlines the scope and objectives of the present study.

Chapter 3:Chapter three presents the experimental investigation of PEG-6000 based finned heat sinks for thermal management applications. Here, efforts have been made to study the effect of heat sink configuration, heat flux, and additive concentration on the thermal performance of PCM based heat sinks.

Chapter 4: Conclusions obtained from present experimental investigations are presented in this chapter. The scope of further investigation is also discussed.

Chapter 3

Experimental investigations into the thermal performance of phase change material-based finned heat sinks for thermal management applications

3.1 General background

Modern electronics components are smaller and more technologically advanced, which increases their power density. In such scenario, it is crucial to design and develop an advanced and reliable cooling module that can dissipate the excess heat and maintain the component at safe operating temperature. Recently, passive cooling based on phase change material (PCM) has emerged as a novel cooling strategy to dissipate heat in the modern electronic devices with intermittent applications. When the PCM integrated heat sink comes in contact with high/low temperature sources, it absorbs/releases thermal energy, changes its phases, and maintains constant temperature [90]. Because of its inherent characteristics of isothermal phase change and high energy storage density, PCM can be used in many applications like thermal and solar energy storage, thermal management of portable electronic systems, heat pipes, outdoor telecommunications enclosures, and battery thermal management [91,92]. However, PCMs possess lower value of thermal conductivity and limits its use in thermal management systems; numerous methods such addition of nanoparticles, metallic foams, and metallic fins have been adopted to enhance the thermal conductivity of heat sinks based on PCM [93,94].

Here, a systematic study has been carried out to analyse the thermal performance of PCM-based heat sinks with plate fin arrangement.

Effect of various numbers of fins (1, 2, 3, and 4) formed by plate fin arrangement, and effect of different heat flux values (2.0-3.0 kW/m²) on the thermal performance is analysed. Also, efforts have been made to analyse the thermal performance of different heat sink configurations such as heat sink with one cavity (HSOC), heat sink with four cavities (HSFC), heat sink with nine cavities (HSNC), and heat sink with sixteen cavities (HSSC) integrated with PCM and CPCM for a varied range of additive concentration (0.5 wt%, 1.0 wt%, and 2.0 wt%) and different heat flux values ($q''=1.7$ kW/m² and 2.4 kW/m²).

3.2 Experimental setup and methodology

Figures 3.1 and 3.2 present the illustrative and photographic view of the test facility, respectively. The test facility includes the heat sink assembly, DC power source (Make: Aplab, Model: L3260), data acquisition system (Make: Agilent, Model: 34972A), k-type thermocouples, and a computer. The heat sink assembly has an aluminum heat sink, plate heater and glass wool insulation to protect heat loss to surroundings. The plate heater's size measures 100×100×4 mm³ and is powered by a DC power supply system that can deliver current and voltage ranging from 0 to 60 A and 0 to 32 V, respectively. To facilitate maximum heat transfer and reduce the thermal contact resistance between the plate heater and the heat sink base, highly conductive thermal paste ($k = 1.27$ W/m.K, HALNZIYE, Shenzhen, China) is used. Owing to higher value of thermal conductivity, low density, corrosion resistance, and lightweight Aluminium-6061 is utilized for fabrication the heat sinks. In the present study, the temperature is recorded by employing the calibrated k-type thermocouples with a data acquisition system that measures the data with frequency of 10 seconds. The thermocouples are attached to the heat sinks in slots made on the sides and the bottom of the heat sinks. The slots have a dimension of 1.5 mm in depth and 1.5 mm in width (Fig. 3.3). There are 14 thermocouples used in the experiment, with 4 placed at the

base and 4 at the side walls of the heat sink. Additionally, 2 thermocouples are located on the plexiglass top, and 1 is positioned at plate heater base. To estimate the amount of heat loss, 2 thermocouples are pasted on the outer surface of insulation. Also, to gauge the temperature of the surroundings, 1 thermocouple bead is left exposed to ambient conditions.

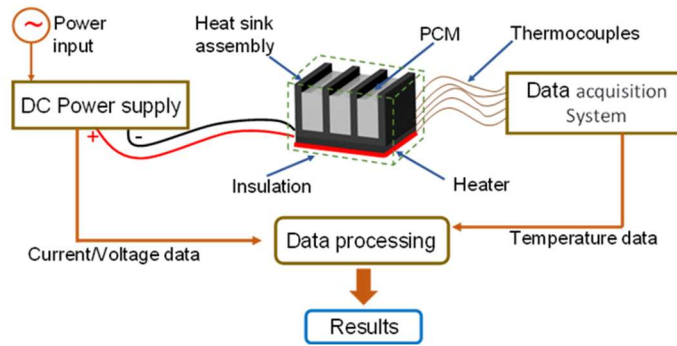


Fig. 3.1 Illustrative representation of the experimental setup

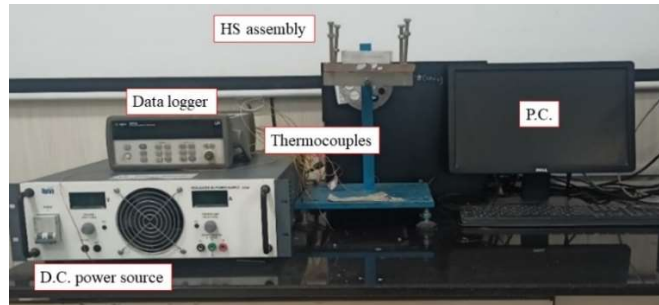
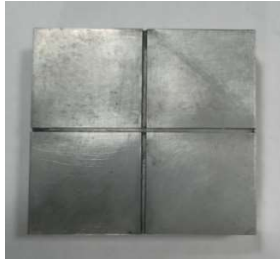


Fig. 3.2 Photographic view of the experimental setup

In the present study, Polyethylene glycol-6000 (Thermo Fisher Scientific, USA), having a melting range of 60-63 °C is used. PEG-6000 is employed as the PCM of choice because of various favorable thermophysical and chemical properties such as congruent melting, high specific heat capacity, and enthalpy of fusion on a volumetric basis, corrosion-resistant, thermally, and chemically stable and non-toxic.



(a)



(b)

Fig. 3.3 Photographic view of slots for placing the thermocouples (a) bottom of the heat sink and (b) side of the heat sink

Table 3.1 Thermophysical properties of various materials [95]

Properties	PEG-6000	EG	MWCNT	Aluminium	Ceramic wool	Plexiglass
Melting temperature (°C)	66.15	-	-	660.37	-	-
Thermal conductivity (W/m.K)	0.2095	300	3000	218	0.12	0.19
Specific heat (kJ/kg.K)	2.374	0.7	0.75	0.896	-	1.470
Latent heat (kJ/kg)	190.44	-	-	-	-	-
Density (kg/m³)	1200	1300	1750	2719	128	-

In order to provide insulation and prevent leakage from the heat sink, plexiglass sheet (4 mm thickness) is used from the top. Table 3.1 summarizes the thermophysical parameters of PEG-6000 (PCM), EG, MWCNT, aluminium (TCE), ceramic wool (insulator), and plexiglass (heat sink enclosure). In the present study, the heat flux is adjusted within

the range of 1.7 kW/m^2 to 3.0 kW/m^2 , which is consistent with the heat flux values typically observed in modern electronic devices. Electrical power is provided by a DC power supply to the plate heater.

3.2.1 Heat sink configurations

The present experimental study aims to investigate the thermal characteristics of different PCM based heat sink configurations. Because of its superior thermal conductivity, low density, corrosion resistance, and lightweight, aluminum is chosen as the heat sink material. Initially, heat sinks with plate fin with PEG-6000 as PCM are considered for study in thermal management applications. The heat sinks used have an overall dimension of $100 \times 100 \times 25 \text{ mm}^3$.

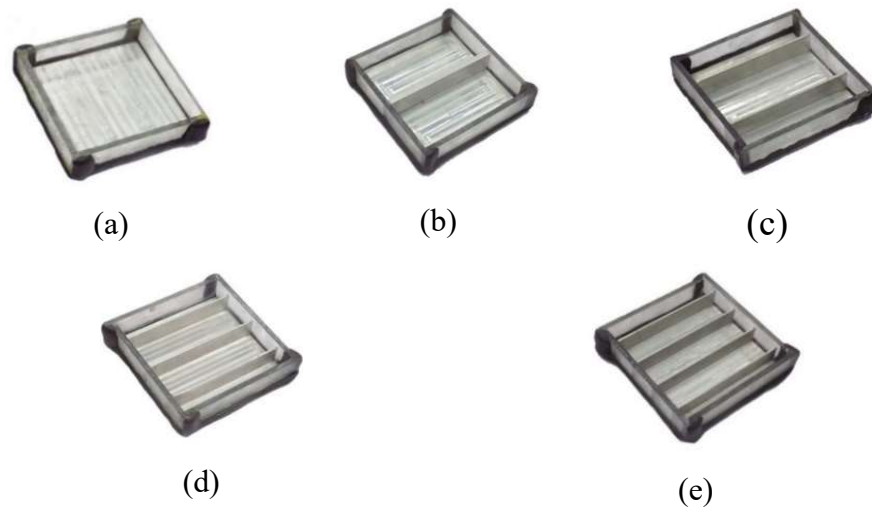


Fig. 3.4 Different heat sink configurations (a) HSNF, (b) HSOF, (c) HSTF, (d) HSTHF, and (e) HSFF

The photographic view of heat sinks used are shown in Fig. 3.4(a-e). All four sides and the top surface of the heat sink are covered with a 5 mm thick transparent plexiglass sheet which also acts as an insulator. The dimensions of various fins utilized in the heat sinks are listed in Table 3.2.

Table 3.2 Fin dimensions of the heat sinks in use [96]

S. No.	Heat sink configuration	Dimensions of fin (mm× mm×mm)
1.	Heat sink with one fin (HSOF)	100×4.25×20
2.	Heat sink with two fin (HSTF)	100×2.12×20
3.	Heat sink with three fin (HSTHF)	100×1.41×20
4.	Heat sink with four fin (HSFF)	100×1.06×20

A study has also been carried on PCM and composite PCM based cross-finned heat sinks. The photographic view of the heat sinks is presented in Fig. 3.5 (a-d). The fins are varied in dimensions to keep a constant volume fraction of 6.60 % in the heat sinks. The overall dimensions of various configurations of cross-finned heat sinks are presented in Table 3.3.

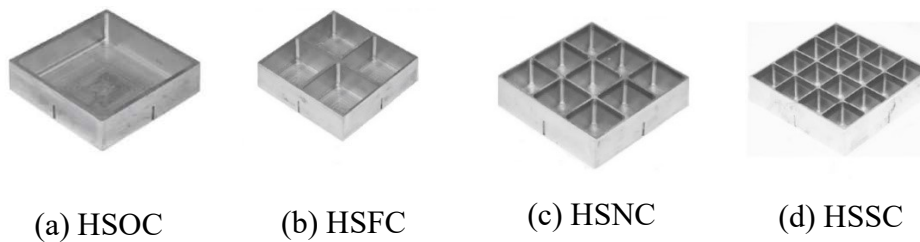


Fig. 3.5 Photographic view of various heat sinks (a) HSOC, (b) HSFC, (c) HSNC, and (d) HSSC

Table 3.3 Dimensions of the heat sinks [50]

Heat sink configuration	Exterior dimensions (mm×mm×mm)	Interior dimensions (mm×mm×mm)	Thickness of fins (mm)	Surface area to volume ratio
HSOC	100×100×25	93×93×23	-	-
HSFC	100×100×25	46.5×46.5×23	3.0	0.043
HSNC	100×100×25	31×31×23	1.5	0.086
HSSC	100×100×25	23.25×23.25×23	1.0	0.129

3.2.2 Uncertainty and heat loss in measurement

In the present experimental study, temperature measurements at different locations are measured using pre-calibrated K-type (chromel-alumel) thermocouples. The Thermocouples are calibrated for the temperature range of 20 to 100 °C following the ASTM standard. A constant temperature bath along with standard mercury in a glass thermometer having a temperature range of 0 to 200 °C and 0.1 °C resolution is used for the calibration of the thermometer. The calibration is performed by immersing one end of all thermocouples into water inside a constant temperature bath, and the other end is connected to the data acquisition system (Make: Agilent, Model: 34972A). The temperature data measured by thermocouples are processed and recorded by a data acquisition system connected to the computer. The immersion heater inside the water bath is used to provide necessary heat to the water, and continuous stirring is carried out to maintain the uniform temperature inside the water bath. Subsequently, the temperature rise of water is measured by a thermometer and the thermocouples after a fixed time interval of 5 min. When the water temperature reaches 100 °C, the electric power source is turned off.

Subsequently, the drop in the temperature of the water is measured at regular intervals. The maximum deviation in the temperature measurement is found to be 0.5 °C.

A standard digital multimeter (Make: Fluke, Model: 287) is used to verify the current and voltage readings of the DC power supply. The measured deviation in the measurement of current and voltage ± 0.1 A and ± 0.1 V, respectively. The uncertainty in the measurement of heat flux is calculated by using the approach proposed by Coleman and Steele [1]. The maximum and uncertainty in heat flux calculation is found to be 5.18%. The Fourier's law for heat conduction can be used to calculate the heat loss as follows: [2]

$$Q_{loss} = \frac{k_{ins} * \Delta T}{\Delta z} \quad (1)$$

where, Q_{loss} is the heat loss through the insulation, k_{ins} is the thermal conductivity of insulation material (0.12 W/m.K), ΔT is the temperature difference between the two insulation surfaces, and Δz (0.025 m) is the thickness of the insulation layer. The temperature difference is calculated from the temperature data collected by using different thermocouples employed on both sides. Based on the temperature values of thermocouples ($T_{13}-T_{14}$), the heat loss to the surroundings is calculated, and the maximum value is found to be 5.73 % for input heat flux value of 2.4 kW/m².

3.2.3 Preparation of composite PCM (CPCM)

The preparation process for the development of CPCM utilizes two main methods, namely the one-step method and the two-step method. Simple mixing, vacuum impregnation, and ultra-sonication are some of the techniques that are employed in the two-step method. Several authors synthesized CPCM and NePCM by employing multiple steps that include mixing and ultra-sonication of pure PCM and additives [99]. CPCM is

obtained by adding EG and MWCNT additives at different mass percentages inside the pure PCM. In the current study, the EG utilized is characterized by its silvery black powder appearance, average size of less than 20 μm , density of 1.3 g/cm^3 , 99.9% purity, and a specific surface area of 15-25 m^2/g . On the other hand, the MWCNT employed exhibits a black powder appearance, average size ranging from 10-20 nm, density of 1-2 g/cm^3 , 99% purity, and a specific surface area of 90-350 m^2/g . Both the additives are manufactured by Nanoshel. EG and MWCNT possess different thermophysical properties. Specifically, EG has a thermal conductivity of 300 $\text{W}/\text{m.K}$, a specific heat of 0.7 $\text{kJ}/\text{kg.K}$, and a density of 1300 kg/m^3 . In contrast, MWCNT exhibits a higher thermal conductivity of 3000 $\text{W}/\text{m.K}$, a slightly higher specific heat of 0.75 $\text{kJ}/\text{kg.K}$, and a greater density of 1750 kg/m^3 .

Table 3.4 Geometrical specifications and characteristics of expanded graphite (EG) and multi-walled carbon nano-tubes (MWCNT)

Material	Expanded graphite (EG)	Multi-walled carbon nano-tubes (MWCNT)
Appearance	Silvery-black powder	Black powder
Purity	99.9%	99%
Size	<20 μm	10-20 nm
Specific surface area	15-25 m^2/g	90-350 m^2/g
Density	1.3 g/cm^3	1-2 g/cm^3

Initially, the PCM (PEG-6000) in flake/powder form and EG in powder form is weighed on an electronic weighing balance (Wensar PGB 301 Precision Balance) having an accuracy of 0.001 g and subsequently, it is melted on a hot plate at fixed temperature of 90°C. Liquid PCM is then

kept on an ultra sonicator water bath at a constant temperature of 70°C, with ultrasonic frequencies of 40 ± 3 kHz and having an ultrasonic wattage of 150 W. The weighed EG is gradually mixed to the liquid PCM; the mixture is then kept in the magnetic stirrer for 1 hour at 70°C while rotating at 400 rpm. The mixture is subsequently transferred to an ultrasonic probe sonicator, where the mixture is subjected to pulse for 2.5 sec and then a resting period of 5 sec while keeping the power rate of 500 watts. This process is repeated for another 90 mins. Subsequently mixture is transferred to the heat sink, layer by layer, and is allowed to cool and solidify in a vacuum environment to ensure no air bubble is trapped during the sonification process, as air bubbles may hamper the thermal conductivity. Figure 3.6 gives a schematic representation of the process of making CPCM. In case the mixture needs to be reused, sonification using the ultrasonic probe sonicator is performed again under similar conditions to ensure no segregation or sedimentation.

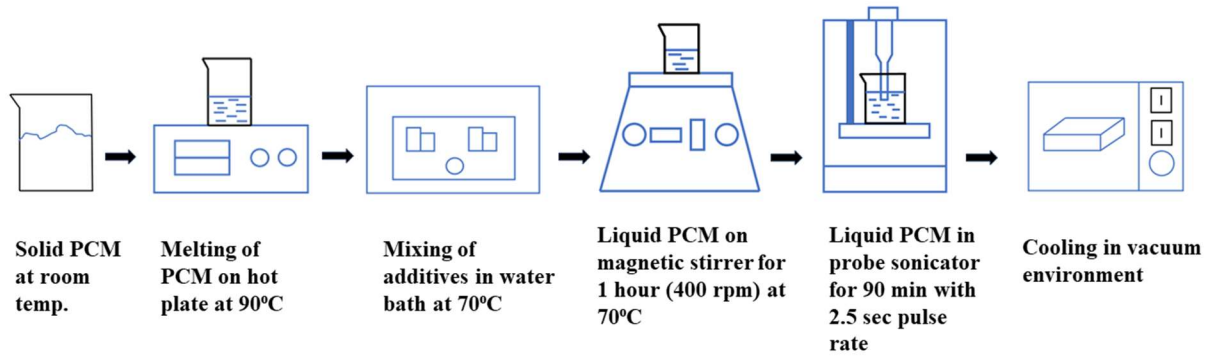


Fig. 3.6 Schematic of the fabrication method of CPCM

3.2.4 Experimental procedure

Solid PCM is first melted in a vacuum furnace and placed into a heat sink container layer by layer, providing enough time for solidification. The process is repeated till the entire heat sink is filled with PCM/CPCM. The filled heat sink is placed in a vacuum oven so that no air pockets exist within the PCM integrated heat sink. Tests are performed at

room temperature and subsequently, the DC power is turned on, and the temperature readings are recorded by using a data acquisition system (Agilent34972A, USA) at regular intervals of 10 s. Heat flux is applied from the DC source by controlling the current and voltage. The heat sink is kept in a horizontal position throughout the experiments for all the cases. Spirit level is utilized to check the horizontal position of the heat sink assembly. Heat input is stopped during the cooling period, and insulations are removed from all the sides except the bottom surface of the heat sink assembly.

3.3 Characterization of PCM and CPCM

3.3.1 DSC analysis of PEG-6000

This experimental study uses polyethylene glycol-6000 (PEG-6000) as the PCM. Various thermos-physical property of the sample for instance latent heat, melting range and specific heat are measured using Differential Scanning Calorimetry (DSC214 Polyma, IIT Indore).

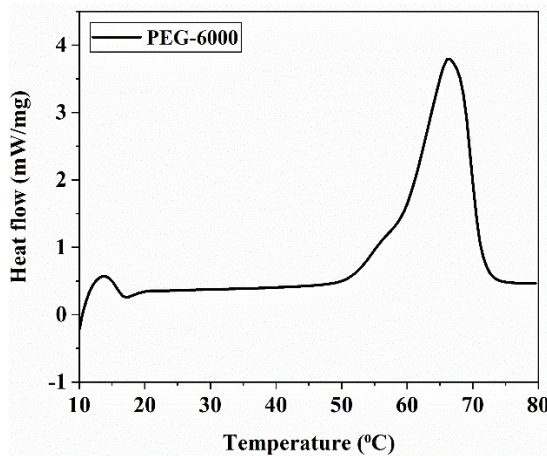


Fig. 3.7 Differential Scanning Calorimetry heating of PEG-6000

Figure 3.7 illustrates the DSC curve of PEG-6000. The DSC testing is carried out at a temperature range of 10 °C to 80 °C, with a heating rate of 10 °C/min. The primary peak depicts the transitioning of phase from solid to liquid which starts at a temp of ~59 °C. It is inferred

from the graph that the beginning, peak point, and termination of the phase transition occurs at 50.73 °C, 66.15 °C and 72.58 °C, respectively. The latent heat of fusion of PCM in use is determined to be 190.44 kJ/kg. The specific heat at the beginning of phase transition is calculated to be 2.374 kJ/kg.K.

3.3.2 DSC analysis of PEG-6000 and composite PCM

DSC analysis of composite PCM (CPCM) are compared in this section. Model: DSC214 Polyma (Make: NETZSCH) is used to obtain the heating and cooling curves having the enthalpy precision varying between $\pm 0.005\%$ to $\pm 0.02\%$. The heating and cooling is conducted at a temperature range of 30-90°C and 70-20°C for the seven samples, Polyethylene glycol-6000 (PEG-6000), PEG-6000+0.5wt% EG (PE1), PEG-6000+1.0wt% EG (PE2), PEG-6000+2.0wt% EG (PE3), PEG-6000+0.5wt% MWCNT (PM1), PEG-6000+1.0wt% MWCNT (PM2), and PEG-6000+2.0wt% MWCNT (PM3). The heating and cooling rate of 10 °C/min is selected to carry out the DSC testing as shown in Fig. 3.8.

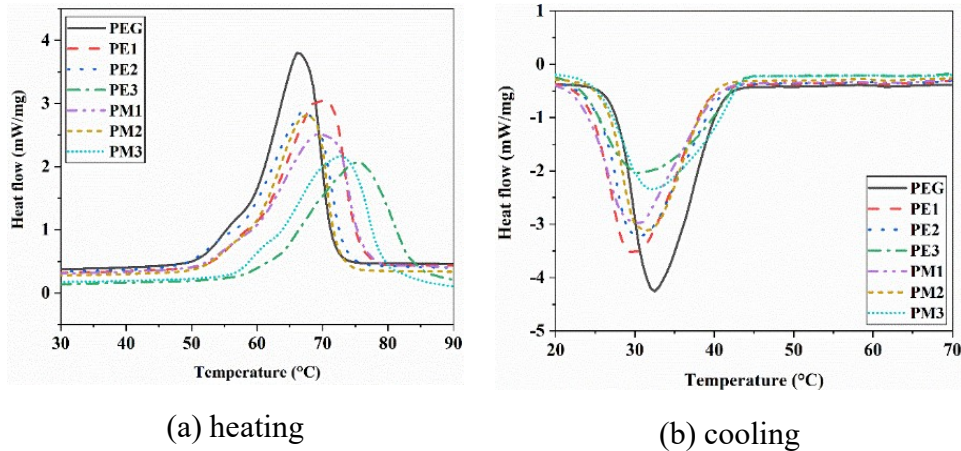


Fig. 3.8 DSC curves comparing PEG-6000 and various CPCMs during (a) heating and (b) cooling

The properties and thermal energy storage characteristics of PEG-6000, PE1, PE2, PE3, PM1, PM2, and PM3 are summarized in Table 4.5.

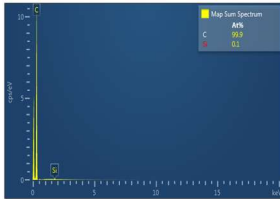
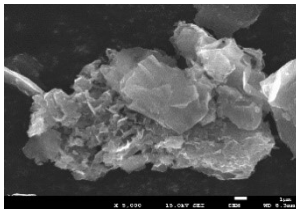
The increment in the peak melting temperature for PE1, PE2, PE3, PM1, PM2 and PM3 is found to be 5.44%, 1.49%, 14.03%, 5.31%, 1.90%, and 10.17%, respectively. On the contrary, the decrease in peak melting temperature is found to be 3.74% and 3.23 % for increase in EG concentration and MWCNT concentration in the CPCM, respectively from 0.5% to 1.0%. For PEG-6000, the calculated specific heat is 2.374 kJ/kg.K and the latent heat is 190.44 kJ/kg. The decrease in specific heat of CPCM is 6.32%, 8.09%, 13.31%, 5.98%, 7.37%, and 14.17% for PE1, PE2, PE3, PM1, PM2 and PM3, respectively. While the decrease in the latent heat of CPCM is found to be 3.49%, 8.25%, 17.69%, 18.26%, 26.65%, and 39.95% for PE1, PE2, PE3, PM1, PM2 and PM3, respectively. The decline in latent heat can be attributed to the fact that the additives do not contribute to the energy storage capacity of the base PCM.

Table 3.5 Thermal energy storage properties of PEG-6000, PEG-6000/EG, and PEG-6000/MWCNT composite PCMs

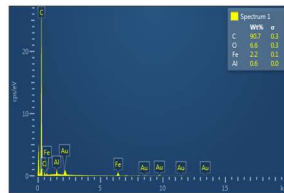
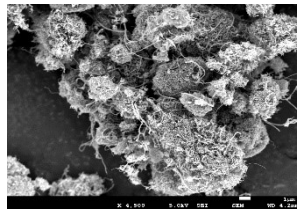
Sample	Melting temperature (°C)	Change in melting temperature (%)	Latent heat (kJ/kg)	Change in latent heat (%)	Specific heat capacity (kJ/kg.K)	Change in specific heat capacity (%)
		$\left \frac{T_{\text{PEG}} - T_{\text{CPCM}}}{T_{\text{PEG}}} \right $		$\left \frac{L_{\text{PEG}} - L_{\text{CPCM}}}{L_{\text{PEG}}} \right $		$\left \frac{C_{\text{PEG}} - C_{\text{CPCM}}}{C_{\text{PEG}}} \right $
PEG-6000	66.15	-	190.44	-	2.374	-
PE1	69.75	5.44	184.02	3.49	2.224	6.32
PE2	67.14	1.49	175.93	8.25	2.182	8.09
PE3	75.43	14.03	161.82	17.69	2.017	13.31
PM1	69.66	5.31	161.04	18.26	2.232	5.98
PM2	67.41	1.90	150.37	26.65	2.199	7.37
PM3	72.88	10.17	136.08	39.95	2.058	14.17

3.3.3 FESEM and EDS analysis of additives and CPCM

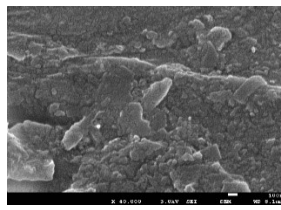
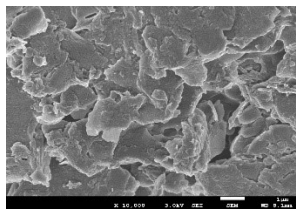
The microparticle and nanoparticle structure, as well as the distribution of additives inside the PCM, are examined using FESEM. Fig. 3.9 shows the FESEM results with the EDS analysis of EG, MWCNT, PEG-6000/EG, and PEG-6000/MWCNT CPCM. From Fig. 3.9 (a) and 3.9 (b), it is seen that EG has layered structure and the image obtained from FESEM shows MWCNT fibers that are intertwined and densely packed together. It can be inferred from the figure that the additives are evenly dispersed throughout the PCM. EDS analysis is a valuable tool in materials characterization, to identify and quantify the elements in a sample. The metallurgical composition of CPCM is investigated using EDS analysis obtained from the FESEM as shown in Fig. 3.9.

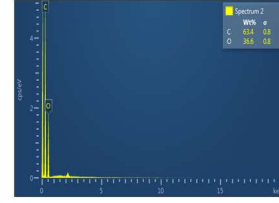
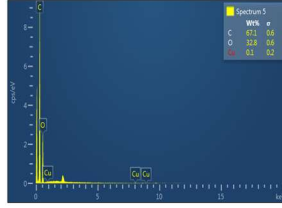


(a) EG



(b) MWCNT





(c) PEG-6000/EG-CPCM (0.5 wt%) (d) PEG-6000/MWCNT-CPCM
(0.5 wt%)

Fig. 3.9 FESEM and EDS analysis of (a) EG, (b) MWCNT, (c) PEG-6000/EG-CPCM (0.5 wt%), and (d) PEG-6000/MWCNT-CPCM (0.5 wt%)

3.3.4 Thermal conductivity measurement of PEG-6000 and CPCM

For thermal conductivity of both PEG-6000 and CPCM, the measurement is carried out using the TEMPOS Thermal Properties Analyzer (manufactured by METER Group) which utilizes the transient line heat source method to make these measurements. The thermal conductivity is measured using a single KS-3 sensor found in the thermal properties' analyzer at room temperature. The estimated thermal conductivity for PEG-6000 is 0.1984 W/m.K whereas the increment in thermal conductivity of CPCM is evaluated to be 6.91%, 18.80%, 29.44%, 16.23%, 40.27%, and 55.80% for PE1, PE2, PE3, PM1, PM2, and PM3, respectively; this observation is similar to the reported studies made by other researchers [65,95]. Figure 3.10 illustrates the enhancement of various CPCMs against PEG-6000.

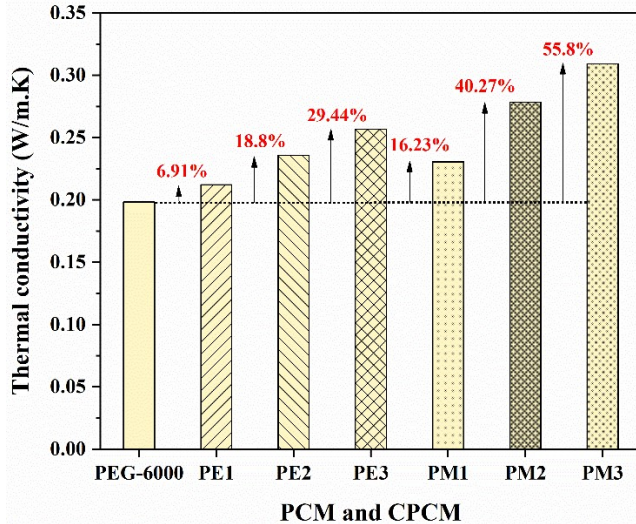
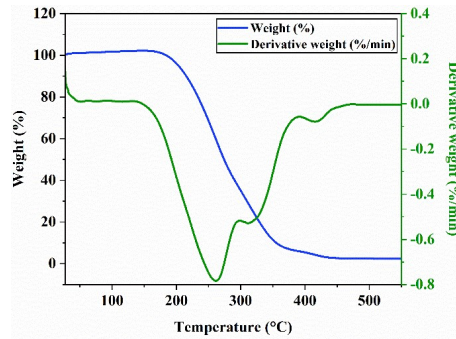


Fig. 3.10 Thermal conductivity enhancement of CPCM

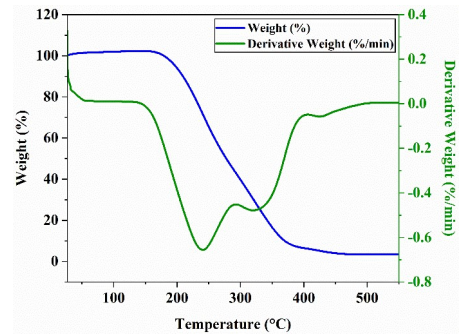
3.3.5 TGA and DTG analysis of PEG-6000 and CPCM

The thermal stability analysis of CPCM is carried out by thermogravimetric analyzer (TGA) (Model: TGA/DSC 1; Make: Mettler Toledo; resolution ~2 micrograms). TGA analysis is particularly useful for studying the degradation and stability of materials under different temperature conditions. The TGA instrument measures the weight of the sample over time and generates a thermogram, which is a plot of the sample mass or weight loss as a function of temperature or time. From the thermogram, several parameters can be determined, including the onset temperature of thermal events, the rate of weight loss, the final residue, and the overall thermal stability of the sample. The thermogravimetric analysis (TGA) depicts the weight loss of the PCM and CPCM (PEG-6000, PE1, PE2, PE3, PM1, PM2 and PM3) at elevated temperature (Fig. 3.11). In addition to the TGA curves, represented by blue colour lines, the derivative thermogravimetric (DTG) graphs are also presented in green colour lines for various CPCMs. The initial and final temperature of decomposition is obtained from the TGA curves, while the DTG curves help to determine the temperature corresponding to the maximum decomposition of CPCM. For TGA, the CPCM are heated from 27 °C to

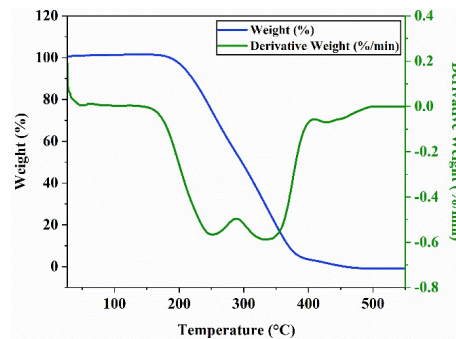
550 °C at a heating rate of 10 °C/min; the results follow a consistent and coherent decomposition process. It can be observed that the decomposition of PCM starts at 168.8 °C and ends at 436.5 °C (Fig. 3.11a). While the decomposition for PE1, PE2, PE3, PM1, PM2, and PM3 starts at 165.5 °C, 175.5 °C, 170.11 °C, 167.8 °C, 168.1 °C, and 176.67 °C and ends at 455.1 °C, 471.1 °C, 443.35 °C, 468.8 °C, 454.1 °C, and 466.47 °C respectively. The temperature for the maximum decomposition rate for samples PCM, PE1, PE2, PE3, PM1, PM2, and PM3 are found to be 260.8 °C, 240.6 °C, 331.6 °C, 272.16 °C, 338.9 °C, 250.3 °C, and 360.65 °C, respectively. It is observed that the decomposition of PCM and CPCMs starts after 160 °C and therefore it can be used for thermal management applications.



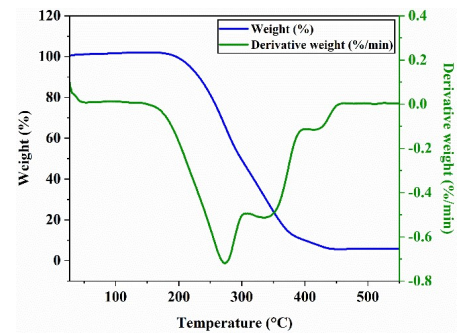
(a) PEG-6000



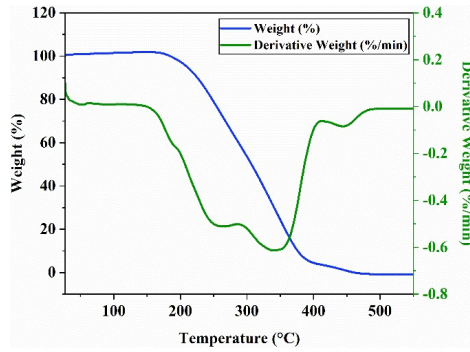
(b) PE1



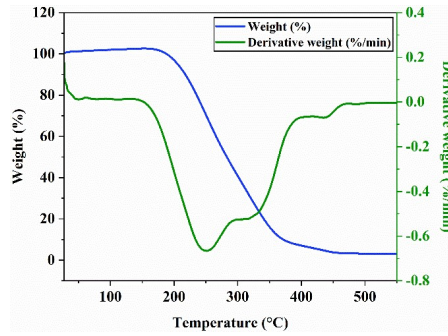
(c) PE2



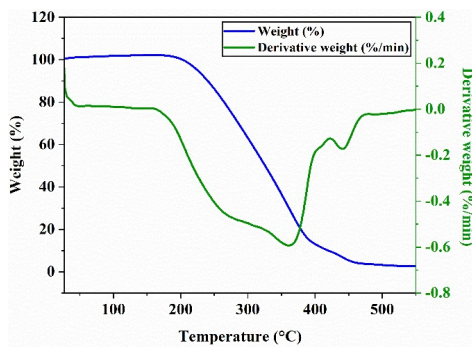
(d) PE3



(e) PM1



(f) PM2



(g) PM3

Fig. 3.11 TGA and DTG analysis of (a) PEG-6000 (b) PE1 (c) PE2 (d) PE3 (e) PM1 (f) PM2, and (g) PM3

3.4 Data reduction

Various parameters namely, additive mass fraction (ϕ), enhancement ratio in operating time (Er), and modified Stefan number (St) are used to study the heat transfer characteristics of different heat sink configurations and CPCM. These parameters are elaborated and defined below.

Additive mass fraction (ϕ): It is defined as the ratio of the mass of additives to the mass of PCM.

$$\varphi = \frac{m_{additives}}{m_{PCM}} \quad (3.2)$$

Enhancement ratio (Er): Enhancement ratio is defined as the time to attain the set-point temperature for the heat sink with PCM (or CPCM) to without PCM for various configurations of heat sinks [50].

$$Er = \frac{\text{time to reach ST with PCM or CPCM}}{\text{time to reach ST without PCM}} \quad (3.3)$$

Modified Stefan number (St): Modified Stefan number is defined as the amount of superheat gained by PCM or CPCM [43].

$$St = \frac{QC}{k_{PCM}L_{PCM}} \quad (3.4)$$

3.5 Results and discussions

3.5.1 Thermal performance analysis of phase change material-based plate finned heat sinks for thermal management applications

This study conducts experiments to investigate the thermal performance of plate fin heat sinks embedded with phase change material (PCM). The plate fin configurations include 1, 2, 3, and 4 fins, as outlined in section 3.2.1. The experiments maintain a constant PCM amount and fin volume, which account for 9% of the total volume in each heat sink design. The heat flux ranges from 2.0 to 3.0 kW/m². Several heat sink configurations, namely HSNF, HSOF, HSTF, HSTHF, and HSFF (illustrated in Fig. 3.4), are examined using an organic PCM, PEG-6000. The study analyzes the impact of heat sink configurations, heat flux, and time taken to reach the set point temperature (ST). The findings are presented through graphs depicting the transient temperature variation of the heat sink base, the time required to achieve the ST, and the enhancement ratio (Er).

Comparison of present study with existing studies

To validate the experimental setup a comparison is done between the present and previous studies. Figure 3.12 compares the current results for temperature variation with time with no fin heat sink with and without the presence of paraffin wax with the existing study of Kumar et al. [65]. A heat flux 2.0 kW/m^2 is supplied to the heat sink assemblage through a plate heater and time-temperature comparison is done.

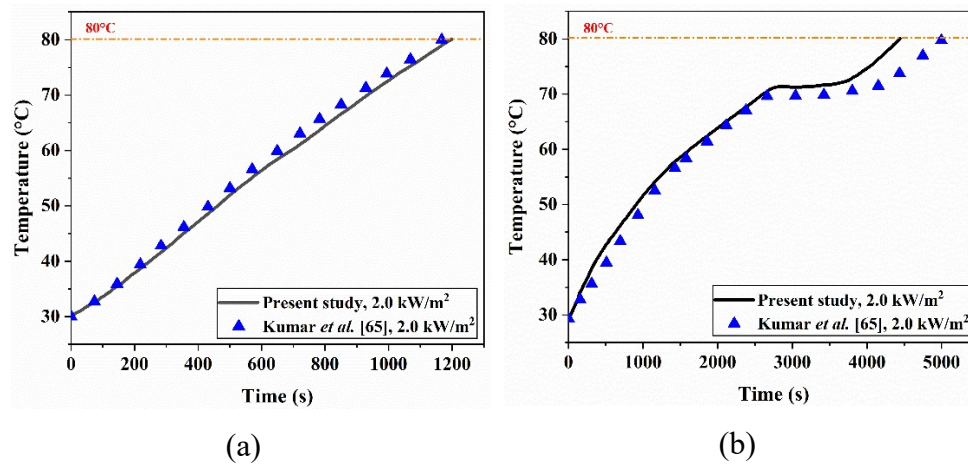


Fig. 3.12 Temperature variation with time for HSNF (a) without PCM, and (b) with PCM

The current investigation's findings demonstrate a pattern that is comparable to that reported in previous experiments done on dimensionally similar heat sink. A slight difference in the validation maybe accounted for the change in ambient conditions i.e., the initial heating temperature.

Effect of heat sink arrangement on the heat sink base temperature

The present investigation is performed at different heat fluxes of 2.0 kW/m^2 , 2.5 kW/m^2 and 3.0 kW/m^2 and the temperature spread over time for various heat sink layouts is shown in Fig. 3.13. The average fluctuation of temperature at the bottom of the heat sink is considered for different values of heat flux as mentioned above. To explore the impact of

different numbers of plate fins on thermal performance, the solid-liquid phase transition of PEG-6000 is compared with different heat flux for five distinct heat sink designs. Figure 3.13 represents the temperature variation with time for various heat sink configurations for varied range of heat flux values.

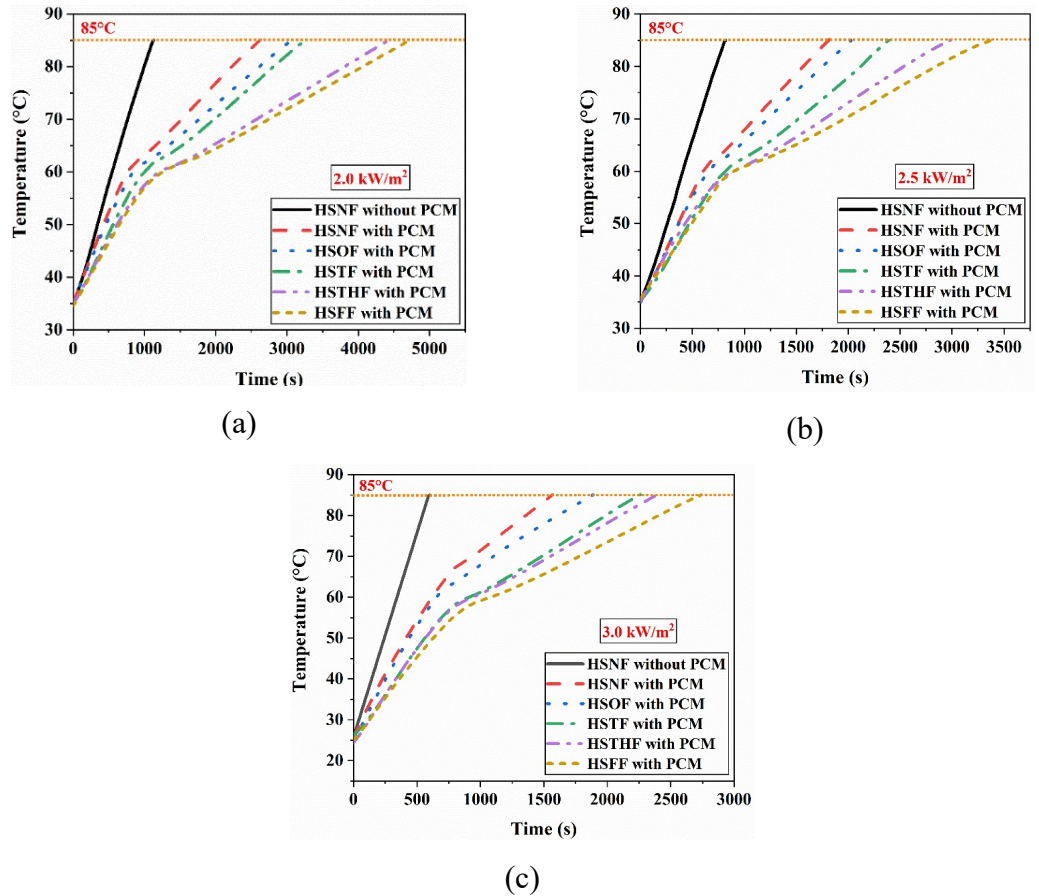


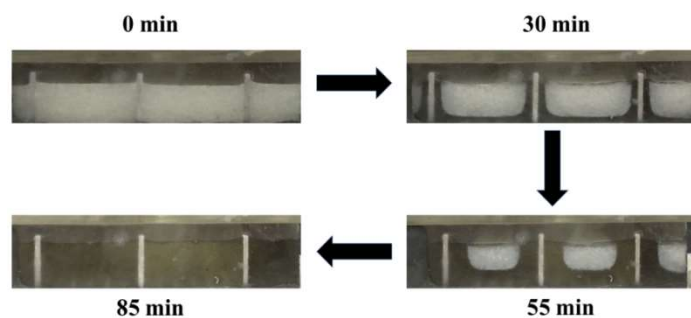
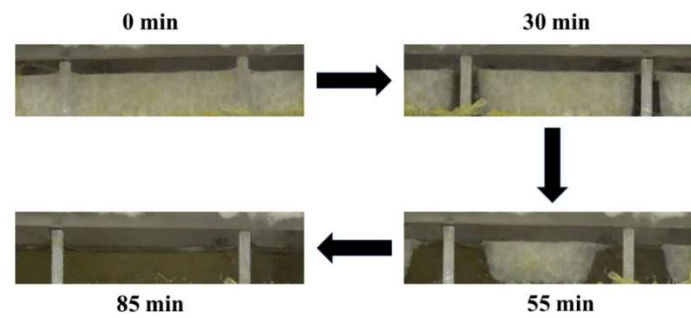
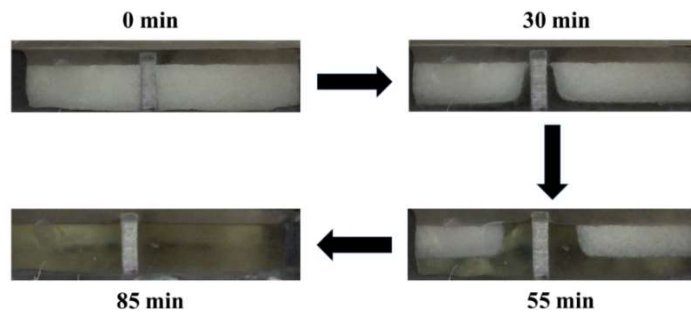
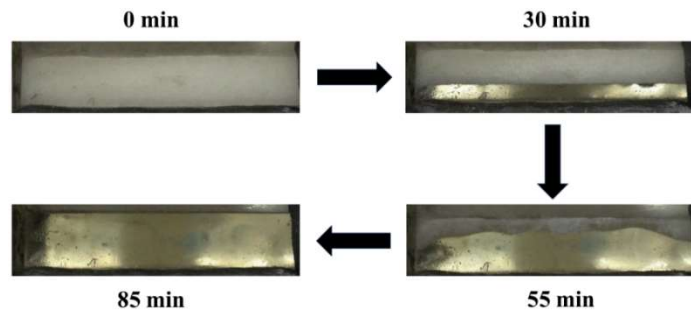
Fig. 3.13 Temperature variation with time for various heat sink layouts at various heat fluxes (a) 2.0 kW/m², (b) 2.5 kW/m², and (c) 3.0 kW/m²

During initial stage of heating, sensible heating takes places and leads to linear variation. While after the initiation of melting the slope of temperature variation changes and takes more time for complete melting. The figures also suggests that with the addition of plate fins in the heat sink, keeping the volume of PCM in all the heat sinks at a constant value, there is a larger surface area for heat transmission and as a result, the heat sink's base temperature remains low and helps in reaching a certain

temperature level at a later point in time. This delay in reaching a certain set point temperature is also due to more uniform melting in heat sinks with fins which helps in better management of temperature of heat sinks possessing plate fins as compared to heat sinks with no fins.

Propagation of melt front in the heat sinks

A digital camera is used in the study to record the propagation of melt front of PCM in successive interval of time. To keep it concise, the images are taken for 3.0 kW/m^2 heat flux at regular intervals for various layouts of heat sinks used in the study. The photographs were captured from the time the PCM is solid until it melts completely. The melting progress is illustrated in Figure 3.14 (a) for HSNF, Figure 3.14 (b) for HSOF, Figure 3.14 (c) for HSTF, Figure 3.14 (d) for HSTHF, and Figure 3.14 (e) for HSFF. The images shown here are considered in a way that it shows a visible difference between consecutive images of propagation of melt front. As seen from the images, there is a difference in melt propagation in case of various configurations of heat sinks. In HSNF, the melt front runs parallel to the bottom plate, whereas in finned heat sinks, the melt front begins near the bottom and runs along the fins before gradually moving towards the centre. This difference between the way melting propagates can be attributed to the number of fins integrated. As more and more fins are added, more area is available for heat transfer and hence melting along with the bottom also occurs near the fins. For the starting few minutes it is observed that melting is slow which can be accounted for the fact that conduction is dominant during the initial phase but as time progresses, convection current sets up and buoyancy forces plays a greater role in the melt propagation of PCM.



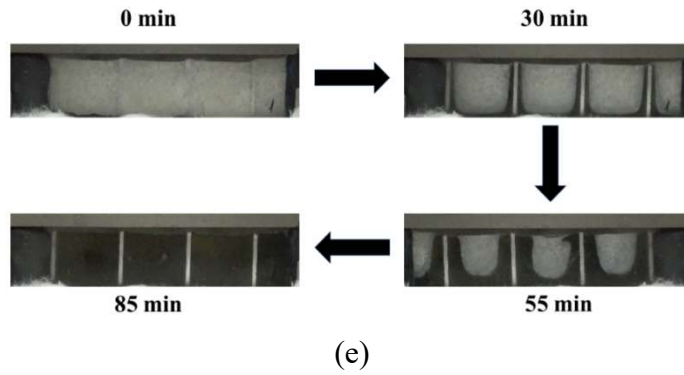
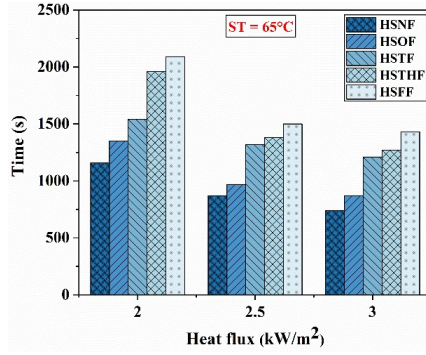


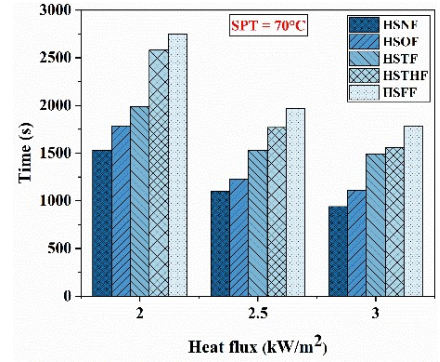
Fig. 3.14 Propagation of melt front for (a) HSNF, (b) HSOF, (c) HSTF, (d) HSTHF, and (e) HSFF

Enhancement ratio (Er) of various heat sinks for different set-point temperatures

Enhancement ratio provides information on stretching the operating time by using different configuration of heat sink. Enhancement ratio is evaluated using the time to attain the targeted temperature for the heat sink with PCM to without PCM for various configurations of heat sinks. In the present experimental study two different set-point temperature, 65 °C and 70 °C, which are critical for optimum functioning of electronic devices are considered and for different heat flux values of 2.0 kW/m², 2.5 kW/m² and 3.0 kW/m². Figure 3.15 shows that when the magnitude of heat flow increases, the time required to reach a critical ST decrease. Also, the time decreases for subsequent variation of heat sinks. In case of set-point temperature (ST) of 65 °C, the decrease in time for HSNF, HSOF, HSTF, HSTHF, HSFF are 420 s, 480 s, 330 s, 690 s, 660s respectively. In case of ST of 70 °C, the decrease in time for HSNF, HSOF, HSTF, HSTHF, HSFF are 590 s, 670 s, 500 s, 1020 s, 970 s, respectively, from a heat flux of 2.0 kW/m² to 3.0 kW/m².



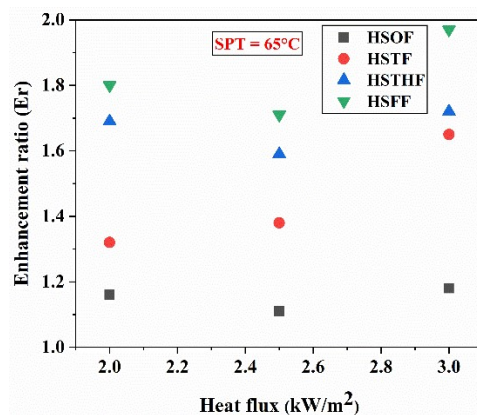
(a)



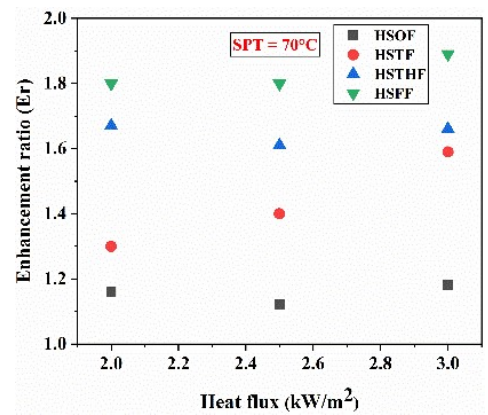
(b)

Fig. 3.15 Time needed to reach critical ST by various layouts of heat sinks for different values of heat flux (a) 65 °C and (b) 70 °C

The enhancement ratio, which is the ratio of time to reach a critical ST by PCM based heat sink with TCE to PCM based heat sink without TCE, is used to describe the decrease in time for various heat sink layouts in this study. The enhancement ratio for a 65 °C and 70 °C critical ST at different heat flux is represented in Fig. 3.16. It can be noted from the graphs that for both critical STs, HSFF gives the highest value of enhancement ratio. In HSFF, a maximum enhancement ratio of 1.97 is obtained for a critical ST of 65 °C and a maximum enhancement ratio of 1.89 is obtained for a critical ST of 70 °C.



(a)



(b)

Fig. 3.16 Enhancement ratio for various layouts of heat sink with different values of heat flux at ST of (a) 65 °C and (b) 70 °C

3.5.2 Investigation of finned heat sinks with PEG-6000/EG and PEG-6000/MWCNT composite phase change material for thermal management application

This study conducts experiments to investigate the thermal performance of cross fin heat sinks embedded with PCM and CPCM. The cross-fin configurations include 1, 4, 9, and 16 cavities, as outlined in section 3.2.1. The experiments maintain a constant PCM amount and fin volume, which account for 6.60 % of the total volume in each heat sink design. The heat flux used is 1.7 and 2.4 kW/m². Several heat sink configurations, namely HSOC, HSFC, HSNC, and HSSC (illustrated in Fig. 3.5), are examined using an organic PCM, PEG-6000. EG and MWCNT are used carbon-based additives to enhance the thermal conductivity of PEG-6000. The study analyzes the impact of heat sink configurations, heat flux, additive concentration, and time taken to reach the set point temperature (ST). The findings are presented through graphs depicting the transient temperature variation of the heat sink base, the time required to achieve the ST, enhancement ratio (Er), and modifies Stefan number (St).

Comparison of present study with existing studies

It is essential to carry out the validation of the test facility with the existing test data. Here, comparison of present results on HSOC without and with PCM are presented with findings of Kumar et al. [65], Ali [63], Kothari et al. [95], Mahmoud et al. [48], Rehman et al. [100] and is shown in Fig. 3.17 (a). It may be noted that Kumar et al. [65], and Kothari et al. [95] used organic PCM (paraffin wax, melting temperature 58-62°C) with a heat sink of dimensions 100 × 100 × 25 mm³. While Ali [63] employed NePCM in a heat pipe set-up with dimension 120 × 120 × 25 mm³ having RT-35HC as base PCM and graphene oxide as nanoparticle. In their study, Mahmoud et al. [48] used paraffin wax in a heat sink of dimension 50 × 50 × 25 mm³ and Rehman et al. [100], employed paraffin wax, RT-35HC,

and RT-44HC as PCM with heat sink of dimension $100 \times 100 \times 25 \text{ mm}^3$. Additionally, the test data of Kumar et al. [65], Kothari et al. [95], Mahmoud et al. [48], Baby et al. [101], and Huang et al. [102] are also compared in Fig. 3.17 (b). In their study, Baby et al. [101] used n-eicosane and paraffin wax with heat sink dimension of $60 \times 42 \times 25 \text{ mm}^3$, while Huang et al. [102] used Lauric acid as PCM on a heat sink dimension of $120 \times 120 \times 35 \text{ mm}^3$. Figures 3.17 (a-b) indicate a similar trend of the heat sink base temperature observed in the current test results and as reported in the previous studies. The deviation in the results can be attributed to the fact that the design and dimensions of heat sinks and use of different PCM in the experiments.

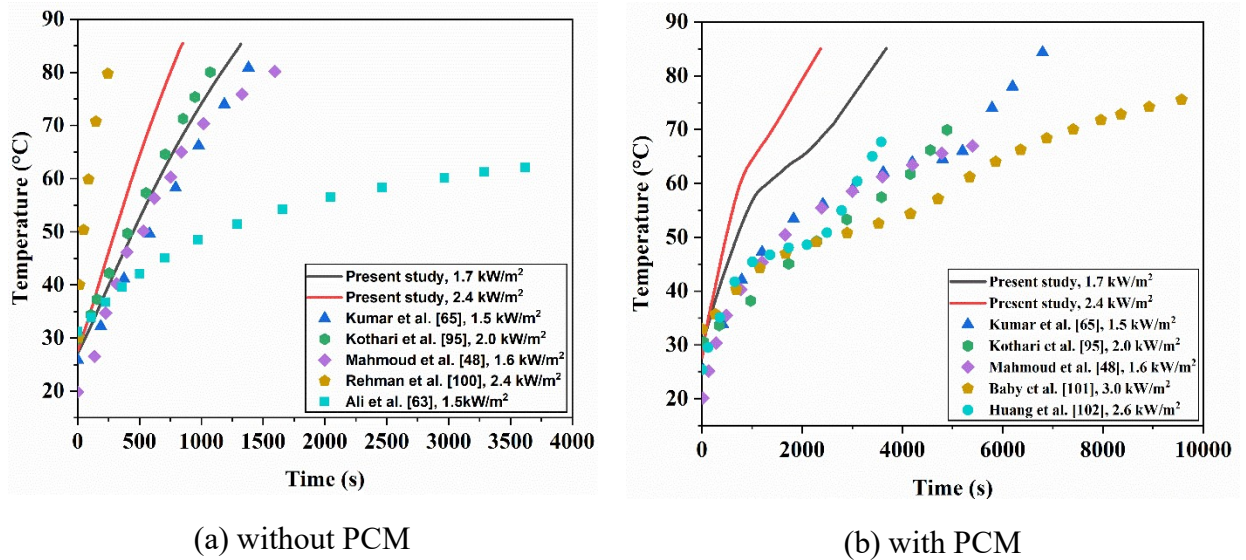


Fig. 3.17 Comparison of present experimental results with the results of other researchers for (a) Heat sink without PCM and (b) Heat sink with PCM

Thermal performance of heat sinks

The temperature-time characteristics for HSOC with and without PCM are depicted in Fig. 3.18. It may be noted that the time to reach maximum operating temperature is of paramount importance in thermal management, hence a target set-point temperature (ST) of 85 °C, which is more than the phase change temperature of PCM and CPCM is used for

the analysis. For $q'' = 1.7 \text{ kW/m}^2$, the time to reach the ST of $85 \text{ }^\circ\text{C}$ is found to be 1320 s and 3680 s by using the HS without and with PCM, respectively; one can notice, the increase in time to attain ST value of $85 \text{ }^\circ\text{C}$ for HS with PCM is 178.8 %. For $q'' = 2.4 \text{ kW/m}^2$, corresponding operating time is 840 s and 2370 s, respectively for HS without and with PCM, respectively; provides an increase in operating time of 182.14 % for ST value of $85 \text{ }^\circ\text{C}$. Extending the time required to reach the ST of $85 \text{ }^\circ\text{C}$ helps to mitigate the adverse effects that may arise due to the increase in temperature when PCM is not used. The PCM offers excellent heat absorption capacity and helps to increase the operating time to reach the targeted temperature.

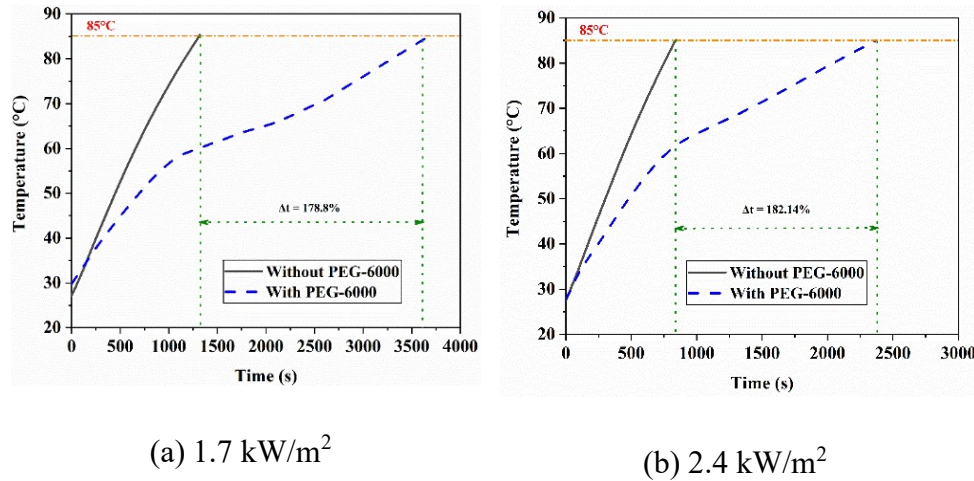
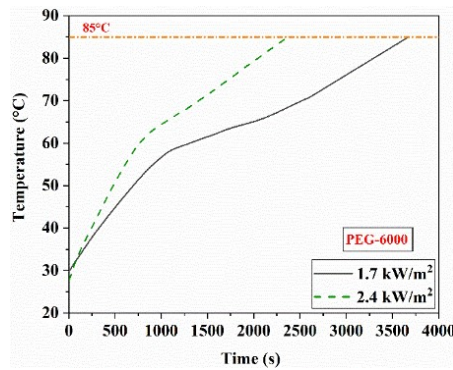


Fig. 3.18 Temperature variation with time for an unfinned heat sink for (a) $q'' = 1.7 \text{ kW/m}^2$ and (b) $q'' = 2.4 \text{ kW/m}^2$

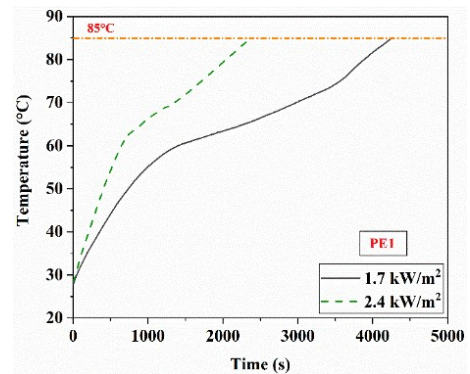
Effect of heat flux

Figure 3.19 illustrates the influence of heat flux on the performance of PCM embedded heat sinks. For the sake of brevity, the investigation is limited to that of PCM, PE1, and PM1 in HSOC. It is observed that on increasing heat flux from 1.7 kW/m^2 to 2.4 kW/m^2 , the duration of latent heating phase decreases considerably. This is due to the fact that in case of higher value of heat flux, more heat is absorbed by the

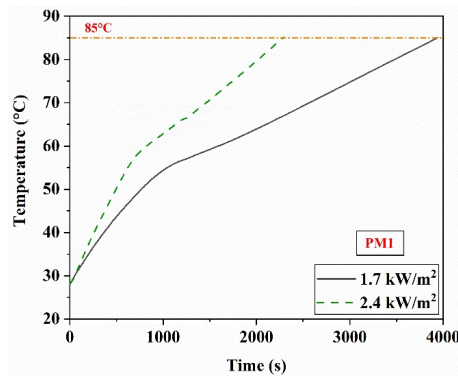
PCM, which results in rapid melting of PCM at an early stage compared to the case for a lower heat flux value. The time taken to reach ST of 85°C for HS with PEG-6000 is found to be 3680 s and 2370 s for $q''= 1.7$ kW/m² and 2.4 kW/m², respectively; while for PE1, the corresponding time is found to be 4260 s and 2380 s and for PM1, the corresponding time is found to be 3940 s and 2290 s, respectively. Similar observations have been made for all heat sinks i.e., HSFC, HSNC, and HSSC and the remaining CPCMs i.e., PE2, PE3, PM2, and PM3.



(a) PEG-6000



(b) PE1



(c) PM1

Fig. 3.19 Time to attain the temperature of 85 °C for heat sink with (a) PEG-6000, (b) PE1, and (c) PM1 for HSOC

Effect of additive concentration

The change in base temperature of the heat sinks with time for various additive concentrations (0%, 0.5%, 1.0%, and 2.0%) and different heat flux values ($q''=1.7 \text{ kW/m}^2$ and 2.4 kW/m^2) are shown in Figs. 3.20-3.21. The capacity to store latent heat in PCM is reduced by the inclusion of additive concentration. For $q''=1.7 \text{ kW/m}^2$, the increment in working time is 17.66 % (PM3), 36.65 % (PE3), 4.4 % (PE3), and 7.07 % (PE3) for HSOC, HSFC, HSNC, and HSSC, respectively.

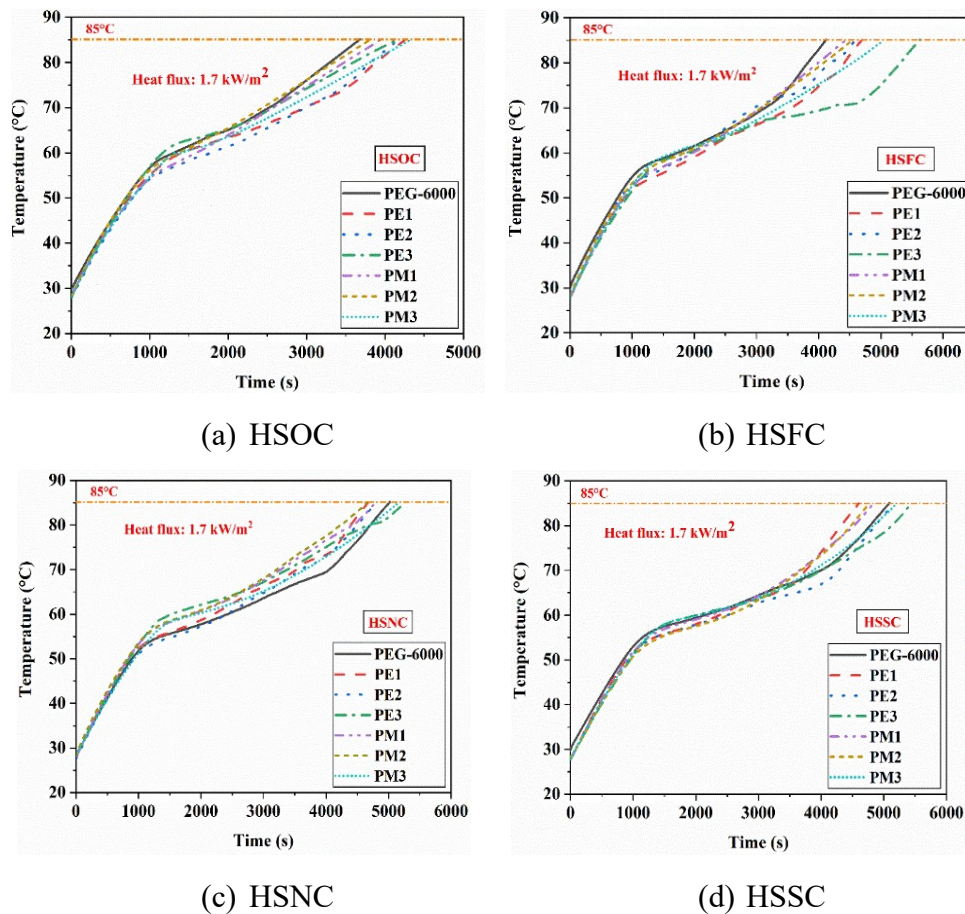


Fig. 3.20 Temperature variation with time to reach a temperature of 85°C at $q''=1.7 \text{ kW/m}^2$ for (a) HSOC, (b) HSFC, (c) HSNC, and (d) HSSC

It is seen that HSFC with PE3 exhibits higher operating time, an increase of 36.65%, as compared to other cases. While, for $q''=2.4 \text{ kW/m}^2$, the increase in operating time is 9.7 % (PM3), 17.54 % (PE3),

11.29 % (PE3), and 4.03 % (PE3) for HSOC, HSFC, HSNC, and HSSC, respectively. It is seen that HSFC with PE3 exhibits higher operating time, an increase of 17.54 %, as compared to other cases.

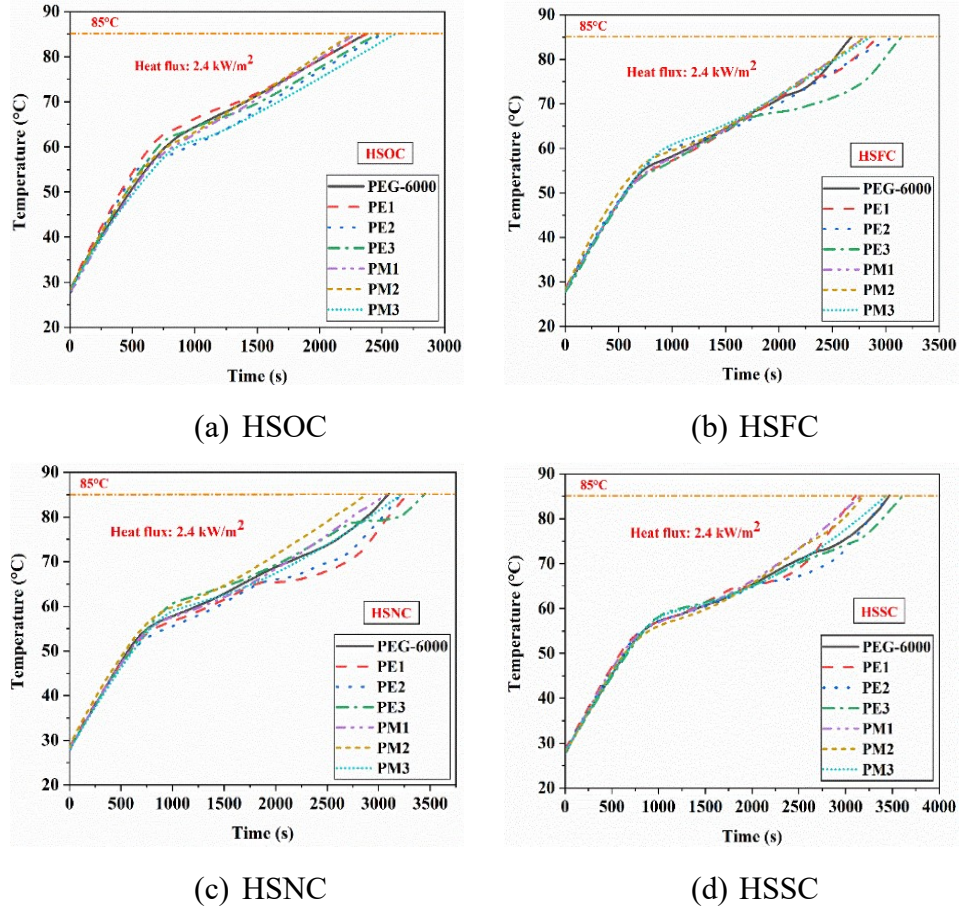
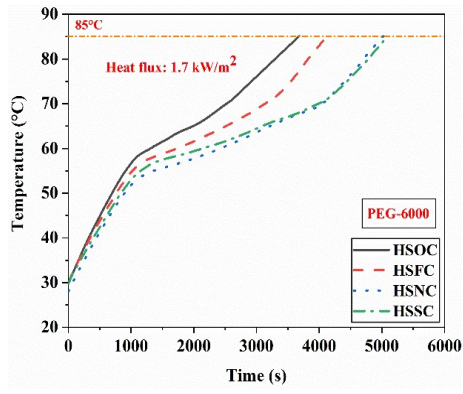


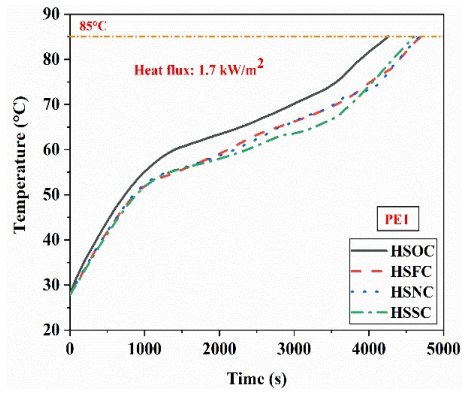
Fig. 3.21 Temperature variation with time to reach a temperature of 85 °C at $q''=2.4 \text{ kW/m}^2$ for (a) HSOC, (b) HSFC, (c) HSNC, and (d) HSSC

Effect of heat sink configuration

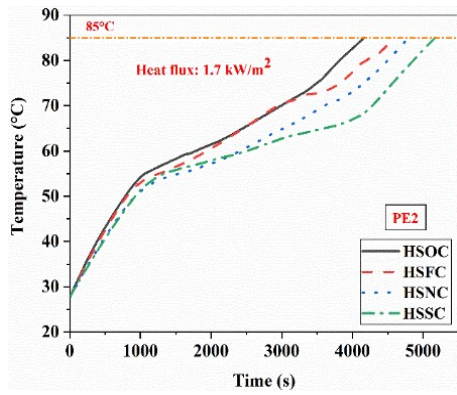
Figs 3.22-3.23 depict the operating time achieved by employing various the heat sinks with PCMs under different heat flux conditions for a ST of 85°C. For $q''= 1.7 \text{ kW/m}^2$, the HSSC involving PEG-6000, PE2, PM1, PM2, and PM3 exhibits the maximum operating time of 5090 s, 5170 s, 4840 s, 4780 s, and 5210 s, respectively; while the corresponding value for HSFC with PE1 and PE3 is found to be 4700 s and 5630 s, respectively (Fig. 3.22).



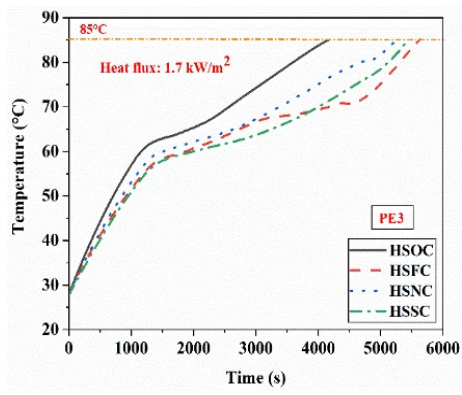
(a) PEG-6000



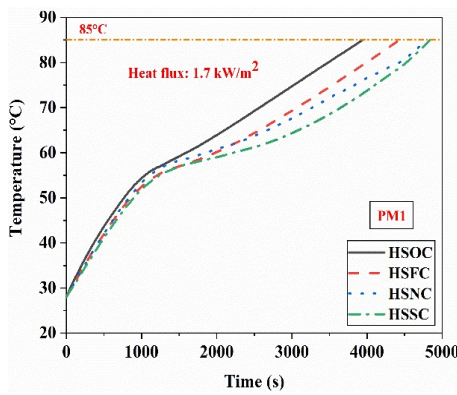
(b) PE1



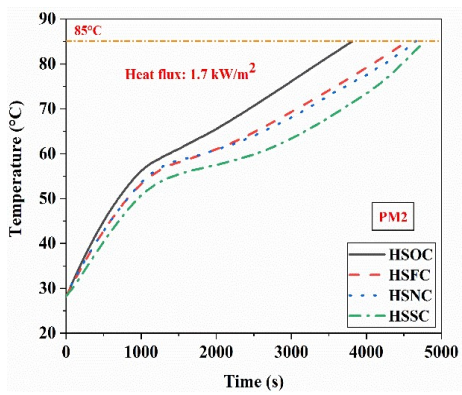
(c) PE2



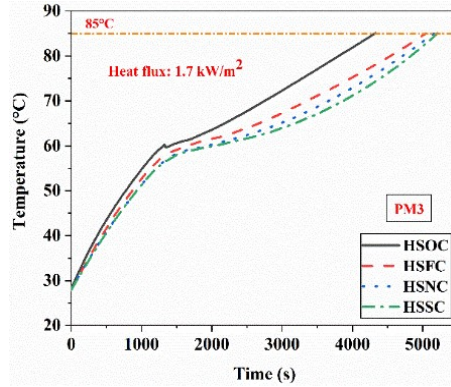
(d) PE3



(e) PM1



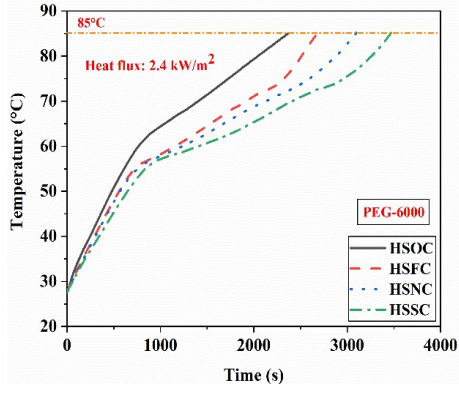
(f) PM2



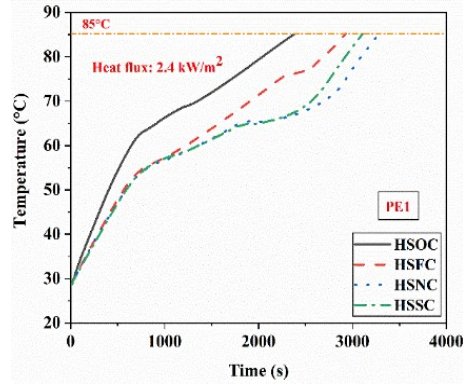
(g) PM3

Fig. 3.22 Temperature variation with time to reach a temperature of 85 °C at $q''=1.7 \text{ kW/m}^2$ for (a) PEG-6000, (b) PE1, (c) PE2, (d) PE3, (e) PM1, (f) PM2, and (g) PM3

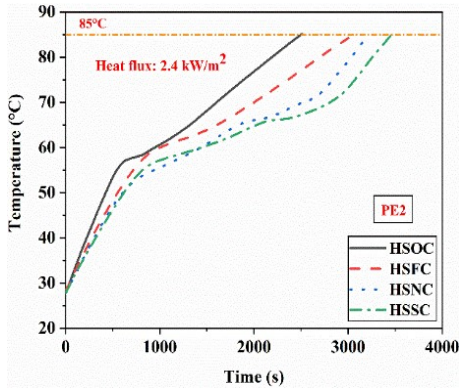
In addition to this, at $q''= 2.4 \text{ kW/m}^2$, the maximum operating time for HSSC with PE2, PE3, PM1, PM2, and PM3 is found to be 3460 s, 3610 s, 3170 s, 3190 sec, and 3430 s, respectively; the corresponding value for HSNC with PE1 is found to be 3280 s (Fig. 3.23). It should be noted that heat is transferred through the base and side walls of heat sink to the PCM; in case of HSOC, the PCM offers high thermal resistance because of the absence of fins and causes poor thermal performance. It is evident from the results that in most of the results HSSC exhibits the superior results for two different values of heat flux; this is attributed to the fact that surface area of fins increases with the fin number resulting in uniform transfer of heat and extracts more heat from the base and walls and maintains a lower value of base temperature for a longer duration of time.



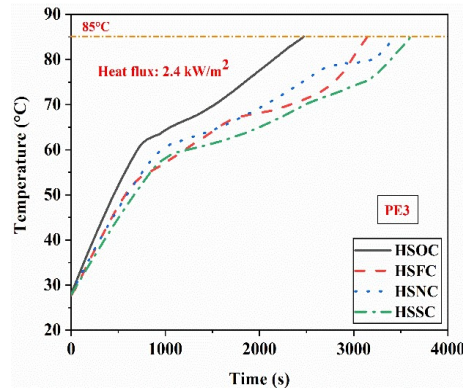
(a) PEG-6000



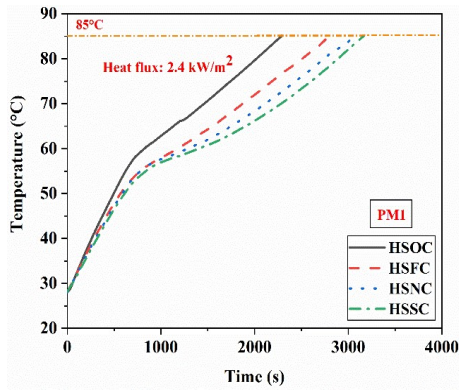
(b) PE1



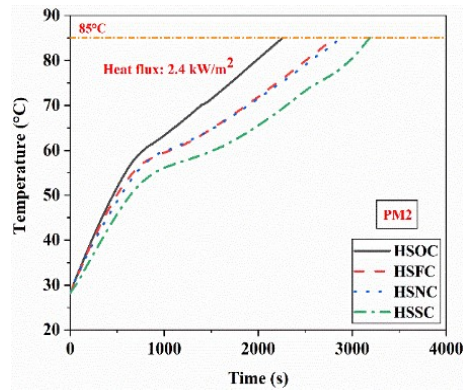
(c) PE2



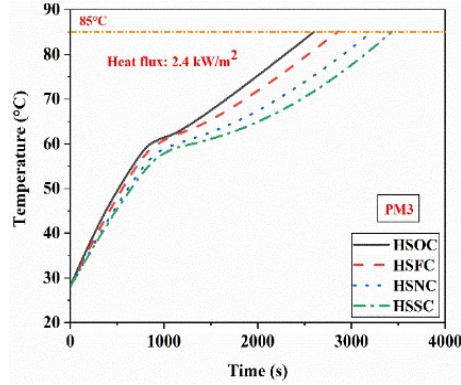
(d) PE3



(e) PM1



(f) PM2

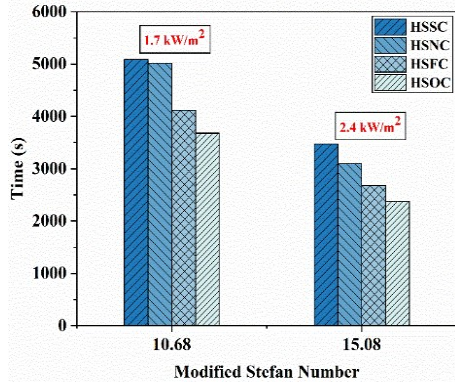


(g) PM3

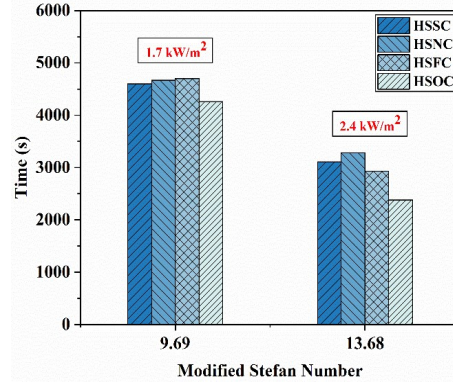
Fig. 3.23 Temperature variation with time to reach a temperature of 85 °C at $q''=2.4 \text{ kW/m}^2$ for (a) PEG-6000, (b) PE1, (c) PE2, (d) PE3, (e) PM1, (f) PM2, and (g) PM3

Modified Stefan Number (St)

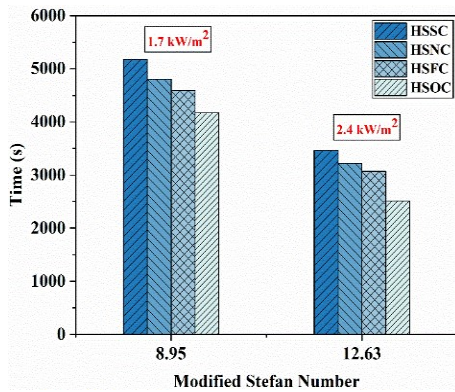
The performance of CPCM is expressed in terms of modified Stefan number. The value of modified Stefan number helps to estimate the heat sinks size based on the heat input and operating time. Figure 3.24 denotes the variation in the Modified Stefan Number with time, which investigates the relative effects of various CPCMs used in the study. The bar graphs represent the time taken by various heat sinks such as HSOC, HSFC, HSNC, and HSSC to reach ST of 85 °C for different heat flux values (1.7 kW/m^2 and 2.4 kW/m^2). Higher St means a higher amount of superheat or lower value of thermal conductivity and latent heat of PCM. An inverse relation is observed between the time and St; as the St increases, the operating time for ST of 85 °C decreases. This indicates that the minimum value of St indicates better thermal performance of the CPCM. The minimum value of St is found to be 8.25 and 11.65 at $q''=1.7 \text{ kW/m}^2$ and $q''=2.4 \text{ kW/m}^2$, respectively for PE3. The heat sinks with longer latent heating phase stretches the operating to reach a given ST value. It is most important to note that the latent heat phase contributes most to stretch the operating period for low values of St.



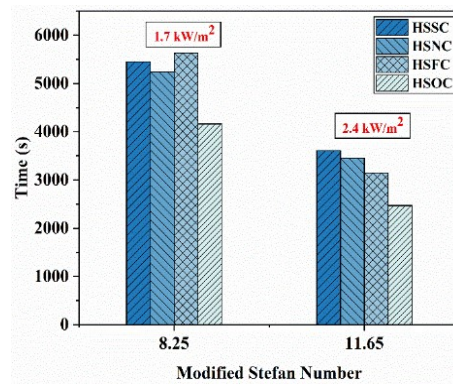
(a) PEG-6000



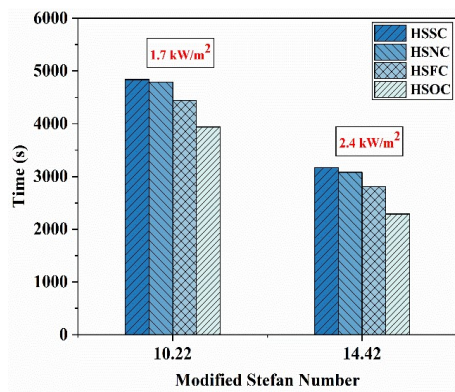
(b) PE1



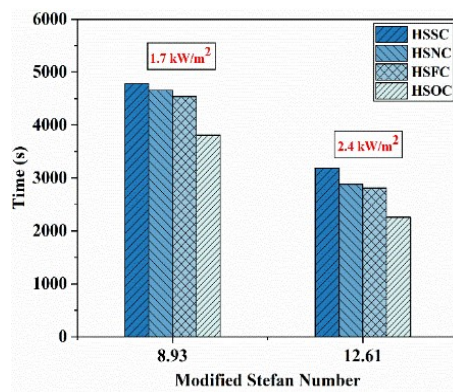
(c) PE2



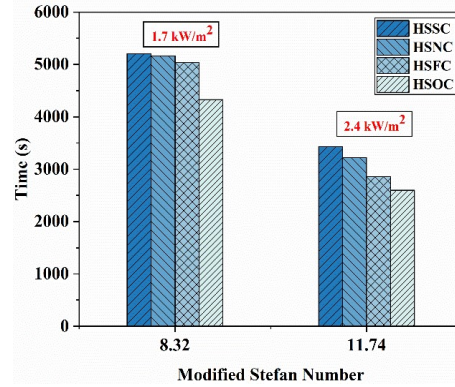
(d) PE3



(e) PM1



(f) PM2



(g) PM3

Fig. 3.24 Comparison of modified Stefan number with time to reach a temperature of 85 °C for (a) PEG-6000, (b) PE1, (c) PE2, (d) PE3, (e) PM1, (f) PM2, and (g) PM3

Enhancement ratio (Er) for various CPCM

This parameter provides information on stretching the operating time by using the phase change composite or different configuration of heat sink. Electronic components operating beyond ST for a longer period may result in degradation of performance and premature failure. Figure 18 represents the enhancement ratio using various CPCM for ST of 85 °C, heat flux and HS configurations. Based on the experimental results, for ST of 85 °C, the highest Er is 1.37 and 1.18 for HSFC with PE3, at $q''=1.7 \text{ kW/m}^2$ and $q''=2.4 \text{ kW/m}^2$, respectively. Based on the results, it can be inferred from the figure that HSFC with PE3 exhibits the best performance for both the heat flux values ($q''=1.7 \text{ kW/m}^2$ and $q''=2.4 \text{ kW/m}^2$) compared to all the cases considered here.

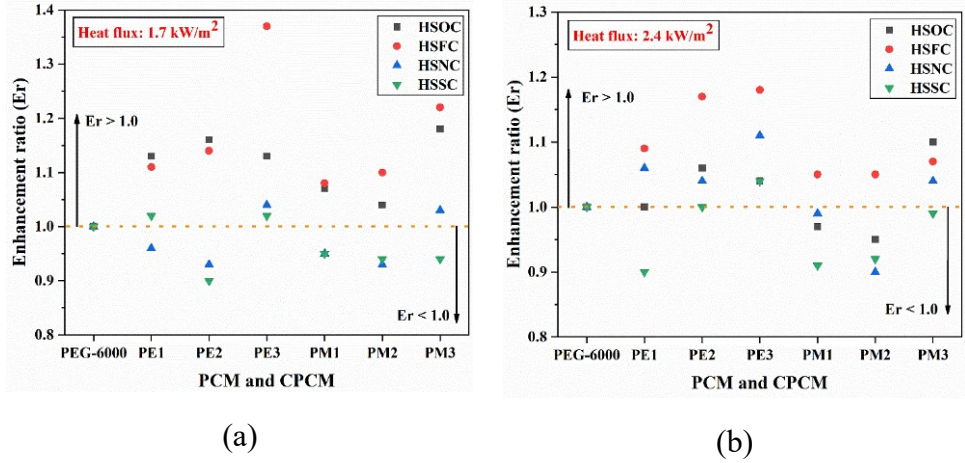


Fig. 3.25 Enhancement ratio at a heat flux of (a) 1.7 kW/m² and (b) 2.4 kW/m² for a ST of 85 °C

3.6 Concluding remarks

Here, tests are conducted to analyse the thermal performance of various PCM-based heat sink configurations. Polyethylene glycol-6000 with melting temperature range 60-63 °C is utilized as PCM. The heat sinks include various thermal conductivity enhancers (TCEs) such as parallel plate fins and cross plate fins. In addition, composite PCM, using EG and MWCNT as additives, is used to evaluate the thermal performance of the heat sink. The effect of fin types, fin arrangements, heat flux values, and additive concentration on the thermal performance is analysed in this chapter. The detailed conclusion of the studies is reported in the next chapter.

Chapter 4

Conclusions and Scope of Future Work

The present dissertation reports the experimental study related to the performance analysis of PCM based heat sink for applications in thermal management. The first problem considers the pure PCM based various plate finned heat sinks for the analysis. While the second study reports the thermal performance of various cross finned heat sinks involving PEG-6000/EG and PEG-6000/MWCNT composites for thermal management applications. Both the analysis incorporates polyethylene glycol-6000 as PCM. The second study makes use of carbon-based microparticle and nanoparticle, expanded graphite (EG) and multi-walled carbon nanotubes (MWCNT), respectively. Effect of various parameters such as different configurations of heat sinks, addition of EG and MWCNT, heat flux, and set-point temperature have been investigated. The significant findings obtained from the present study are elaborated below:

4.1 Thermal Performance Analysis of Phase Change Material-Based Plate Finned Heat Sinks for Thermal Management Applications

The thermal performance of PCM (PEG-6000) based heat sinks was investigated experimentally for five different configurations (HSNF, HSOF, HSTF, HSTHF and HSFF) is performed in this work. The study of the integration of fins into heat sinks is carried out at three different values of heat flux 2.0 kW/m^2 , 2.5 kW/m^2 and 3.0 kW/m^2 and the conclusions from this study are as follows:

- For the same time interval, the PCM melts in the order of HSFF-HSTHF-HSTF-HSOF-HSNF, suggesting more heat transfer when there is an addition of plate fins in the heat sinks.
- A heat sink with plate fins lowers the temperature at the bottom for a longer period of time than a heat sink without fins.

- For a SPT of 65°C, the maximum enhancement ratio obtained is 1.97 for a heat flux of 3.0 kW/m² for HSFF.
- For a SPT of 70°C, the maximum enhancement ratio obtained is 1.89 for a heat flux of 3.0 kW/m² for HSFF.

4.2 Investigating finned heat sinks with PEG-6000/EG and PEG-6000/MWCNT composite phase change material for thermal management application

Thermal performance of various composite phase change material (CPCM) based heat sink configurations are analyzed through experimental investigation. Four heat sink configurations namely, heat sink with one cavity (HSOC), heat sink with four cavities (HSFC), heat sink with nine cavities (HSNC), and heat sink with sixteen cavities (HSSC) are used in this study for different heat flux values namely $q''= 1.7 \text{ kW/m}^2$ and $q''=2.4 \text{ kW/m}^2$; the set point temperature (ST) for all cases is fixed at 85°C for the analysis. The CPCM is synthesized by adding different concentrations by weight (0.5%, 1.0 % and 2.0%) of EG and MWCNT separately with PEG-6000. The thermophysical properties and stability of CPCM are analyzed. The outcomes of the present study are summarized below.

- From the observed properties from different analyses, it is noticed that the thermal properties of CPCMs can be varied with addition of different concentration of additives. The latent heat of the developed material is found to vary between 136.08 kJ/kg-184 kJ/kg, while the thermal conductivity varies between 0.2121 W/m.K - 0.3091 W/m.K. The CPCM exhibited good thermal stability.
- The operating time for ST of 85 °C is found reduce with the increase in the heat flux values for all the heat sink configurations. For HSOC, the reduction in operating time is found to be 35.6%, 44.13% and 41.88% for PEG-6000, PE1, and PM1, respectively with the increase in heat flux from $q''= 1.7 \text{ kW/m}^2$ to 2.4 kW/m^2 .

- The maximum enhancement in operating time with different CPCMs is found to be 17.66%, 36.65%, 4.4%, and 7.07% for HSOC, HSFC, HSNC, and HSSC, respectively at $q''= 1.7 \text{ kW/m}^2$. The HSFC with PE3 exhibits the highest increase in operating time of 36.65% and 17.54% at $q''= 1.7 \text{ kW/m}^2$ and $q''= 2.4 \text{ kW/m}^2$, respectively.
- The minimum value of modified Stefan number (St) indicates better thermal performance of the CPCM. The minimum value of St is found to be 8.25 and 11.65 at $q''=1.7 \text{ kW/m}^2$ and $q''=2.4 \text{ kW/m}^2$, respectively for PE3.
- The maximum value of enhancement ratio is found to be 1.37 and 1.18 for HSFC with PE3 at $q''=1.7 \text{ kW/m}^2$ and $q''=2.4 \text{ kW/m}^2$, respectively.

4.3 Scope of future work

Phase change materials (PCMs) have gained significant interest in recent years due to their unique ability to store and release large amounts of energy during phase transitions. This property makes them highly valuable for various applications, including energy storage, thermal management, and electronics cooling.

The present dissertation reports the experimental study pertaining to the PCM based heat sinks for thermal management applications. Effect of various parameters such as different configurations of heat sinks, heat flux, carbon-based additives, and time to reach a set-point temperature (ST) have been investigated here. The findings obtained in this dissertation can provide valuable information for further investigation in this area. Some of the potential future directions are elaborated here.

- Efforts should be made to develop advanced PCM composite with enhanced thermophysical properties.
- Characterization of composite PCMs should be made to analyse the thermal stability and ensure the required thermal properties.

- Experiments need to be conducted with cascaded PCM based heat sinks to meet the need of variable temperature requirements.
- Numerical study should be performed to analyse the effect of fin shape, arrangement in PCM based system on the thermal performance.

REFERENCES

1. Wang, C., Hua, L., Yan, H., Li, B., Tu, Y., and Wang, R. (2020) A Thermal Management Strategy for Electronic Devices Based on Moisture Sorption-Desorption Processes. *Joule*, **4** (2), 435–447.
2. Abo-Zahhad, E.M., Ookawara, S., Radwan, A., Elkady, M.F., and El-Shazly, A.H. (2020) Optimization of stepwise varying width microchannel heat sink for high heat flux applications. *Case Studies in Thermal Engineering*, **18**.
3. Hosseinizadeh, S.F., Tan, F.L., and Moosania, S.M. (2011) Experimental and numerical studies on performance of PCM-based heat sink with different configurations of internal fins. *Appl Therm Eng*, **31** (17–18), 3827–3838.
4. Yeh, L.T. (1995) Review of Heat Transfer Technologies in Electronic Equipment.
5. Radwan, A., and Ahmed, M. (2017) The influence of microchannel heat sink configurations on the performance of low concentrator photovoltaic systems. *Appl Energy*, **206**, 594–611.
6. Sarbu, I., and Sebarchievici, C. (2018) A comprehensive review of thermal energy storage. *Sustainability (Switzerland)*, **10** (1).
7. Huber, C., Jahromy, S.S., Jordan, C., Schreiner, M., Harasek, M., Werner, A., and Winter, F. (2019) Boric acid: A high potential candidate for thermochemical energy storage. *Energies (Basel)*, **12** (6).
8. Talati, F., Mosaffa, A.H., and Rosen, M.A. (2011) Analytical approximation for solidification processes in PCM storage with internal fins: Imposed heat flux. *Heat and Mass Transfer/Waerme- und Stoffuebertragung*, **47** (4), 369–376.
9. Riffat, S., Mempoou, B., and Fang, W. (2015) Phase change material developments: a review. *International Journal of Ambient Energy*, **36** (3), 102–115.
10. Zhou, D., Zhao, C.Y., and Tian, Y. (2012) Review on thermal energy storage with phase change materials (PCMs) in building applications. *Appl Energy*, **92**, 593–605.

11. Abhat, A. Low Temperature Latent Heat Thermal Energy Storage: Heat Storage Materials. *Solar Ene, Tç~*, **10** (4).
12. Oró, E., de Gracia, A., Castell, A., Farid, M.M., and Cabeza, L.F. (2012) Review on phase change materials (PCMs) for cold thermal energy storage applications. *Appl Energy*, **99**, 513–533.
13. Safari, A., Saidur, R., Sulaiman, F.A., Xu, Y., and Dong, J. (2017) A review on supercooling of Phase Change Materials in thermal energy storage systems. *Renewable and Sustainable Energy Reviews*, **70**, 905–919.
14. Khudhair, A.M., and Farid, M.M. (2004) A review on energy conservation in building applications with thermal storage by latent heat using phase change materials. *Energy Convers Manag*, **45** (2), 263–275.
15. Sahoo, S.K., Das, M.K., and Rath, P. (2016) Application of TCE-PCM based heat sinks for cooling of electronic components: A review. *Renewable and Sustainable Energy Reviews*, **59**, 550–582.
16. Cai, Y., Wang, Y., Liu, D., and Zhao, F.Y. (2019) Thermoelectric cooling technology applied in the field of electronic devices: Updated review on the parametric investigations and model developments. *Appl Therm Eng*, **148**, 238–255.
17. Abokersh, M.H., Osman, M., El-Baz, O., El-Morsi, M., and Sharaf, O. (2018) Review of the phase change material (PCM) usage for solar domestic water heating systems (SDWHS). *Int J Energy Res*, **42** (2), 329–357.
18. Khan, M.M.A., Saidur, R., and Al-Sulaiman, F.A. (2017) A review for phase change materials (PCMs) in solar absorption refrigeration systems. *Renewable and Sustainable Energy Reviews*, **76**, 105–137.
19. Xu, B., Li, P., and Chan, C. (2015) Application of phase change materials for thermal energy storage in concentrated solar thermal power plants: A review to recent developments. *Appl Energy*, **160**, 286–307.
20. Gutierrez, A., Miró, L., Gil, A., Rodríguez-Aseguinolaza, J., Barreneche, C., Calvet, N., Py, X., Inés Fernández, A., Grágeda, M., Ushak, S., and Cabeza, L.F. (2016) Advances in the valorization of waste and by-product materials as thermal energy

storage (TES) materials. *Renewable and Sustainable Energy Reviews*, **59**, 763–783.

21. Nomura, T., Okinaka, N., and Akiyama, T. (2010) Waste heat transportation system, using phase change material (PCM) from steelworks to chemical plant. *Resour Conserv Recycl*, **54** (11), 1000–1006.
22. Shon, J., Kim, H., and Lee, K. (2014) Improved heat storage rate for an automobile coolant waste heat recovery system using phase-change material in a fin-tube heat exchanger. *Appl Energy*, **113**, 680–689.
23. Kim, J., Oh, J., and Lee, H. (2019) Review on battery thermal management system for electric vehicles. *Appl Therm Eng*, **149**, 192–212.
24. Siddique, A.R.M., Mahmud, S., and Heyst, B. Van (2018) A comprehensive review on a passive (phase change materials) and an active (thermoelectric cooler) battery thermal management system and their limitations. *J Power Sources*, **401**, 224–237.
25. Islam, M.M., Pandey, A.K., Hasanuzzaman, M., and Rahim, N.A. (2016) Recent progresses and achievements in photovoltaic-phase change material technology: A review with special treatment on photovoltaic thermal-phase change material systems. *Energy Convers Manag*, **126**, 177–204.
26. Waqas, A., Ji, J., Xu, L., Ali, M., Zeashan, and Alvi, J. (2018) Thermal and electrical management of photovoltaic panels using phase change materials - A review. *Renewable and Sustainable Energy Reviews*, **92**, 254–271.
27. Raj, C.R., Suresh, S., Bhavsar, R.R., Singh, V.K., and Govind, K.A. (2020) Influence of fin configurations in the heat transfer effectiveness of Solid solid PCM based thermal control module for satellite avionics: Numerical simulations. *J Energy Storage*, **29**.
28. Kansara, K., Singh, V.K., Patel, R., Bhavsar, R.R., and Vora, A.P. (2021) Numerical investigations of phase change material (PCM) based thermal control module (TCM) under the influence of low gravity environment. *Int J Heat Mass Transf*, **167**.

29. Dutt Sharma, S., Kitano, H., and Sagara, K. (2004) Phase Change Materials for Low Temperature Solar Thermal Applications. *Res. Rep. Fac. Eng. Mie Univ*, **29**.
30. Henze, R.H., and Humphrey, J.A.C. (1981) Enhanced Heat Conduction In Phase-Change Thermal Energy Storage Devices. *Heat Mass Transfer*, **24**.
31. Sebti, S.S., Mastiani, M., Mirzaei, H., Dadvand, A., Kashani, S., and Hosseini, S.A. (2013) Numerical study of the melting of nano-enhanced phase change material in a square cavity. *Journal of Zhejiang University: Science A*, **14** (5), 307–316.
32. Fan, L., and Khodadadi, J.M. (2012) A theoretical and experimental investigation of unidirectional freezing of nanoparticle-enhanced phase change materials. *J Heat Transfer*, **134** (9).
33. Liu, L., Su, D., Tang, Y., and Fang, G. (2016) Thermal conductivity enhancement of phase change materials for thermal energy storage: A review. *Renewable and Sustainable Energy Reviews*, **62**, 305–317.
34. Yataganbaba, A., Ozkahraman, B., and Kurtbas, I. (2017) Worldwide trends on encapsulation of phase change materials: A bibliometric analysis (1990–2015). *Appl Energy*, **185**, 720–731.
35. Suryanarayana, C., Rao, K.C., and Kumar, D. (2008) Preparation and characterization of microcapsules containing linseed oil and its use in self-healing coatings. *Prog Org Coat*, **63** (1), 72–78.
36. Hassab, M.A., Sorour, M.M., Khamis Mansour, M., and Zaytoun, M.M. (2017) Effect of volume expansion on the melting process's thermal behavior. *Appl Therm Eng*, **115**, 350–362.
37. Zivkovic, B., and Fujii, I. (2001) An Analysis of Isothermal Phase Change of Phase Change Material Within Rectangular And Cylindrical Containers. **70** (1).
38. Ismail, K.A.R., and Batista De Jesus, A. (2001) Parametric study of solidification of PCM around a cylinder for ice-bank applications. *International Journal of Refrigeration*, **24**.
39. Tan, F.L., Hosseinizadeh, S.F., Khodadadi, J.M., and Fan, L. (2009) Experimental and computational study of constrained melting of

- phase change materials (PCM) inside a spherical capsule. *Int J Heat Mass Transf*, **52** (15–16), 3464–3472.
40. Baby, R., and Balaji, C. (2012) Experimental investigations on phase change material based finned heat sinks for electronic equipment cooling. *Int J Heat Mass Transf*, **55** (5–6), 1642–1649.
 41. Baby, R., and Balaji, C. (2013) A neural network-based optimization of thermal performance of phase change material-based finned heat sinks-an experimental study. *Experimental Heat Transfer*, **26** (5), 431–452.
 42. Xu, Y., Wang, J., and Li, T. (2022) Experimental study on the heat transfer performance of a phase change material based pin-fin heat sink for heat dissipation in airborne equipment under hypergravity. *J Energy Storage*, **52**.
 43. Ali, H.M., Ashraf, M.J., Giovannelli, A., Irfan, M., Irshad, T. Bin, Hamid, H.M., Hassan, F., and Arshad, A. (2018) Thermal management of electronics: An experimental analysis of triangular, rectangular and circular pin-fin heat sinks for various PCMs. *Int J Heat Mass Transf*, **123**, 272–284.
 44. Kim, S.H., Heu, C.S., Mok, J.Y., Kang, S.W., and Kim, D.R. (2022) Enhanced thermal performance of phase change material-integrated fin-type heat sinks for high power electronics cooling. *Int J Heat Mass Transf*, **184**.
 45. Baby, R., and Balaji, C. (2014) Thermal performance of a PCM heat sink under different heat loads: An experimental study. *International Journal of Thermal Sciences*, **79**, 240–249.
 46. Arshad, A., Ali, H.M., Khushnood, S., and Jabbal, M. (2018) Experimental investigation of PCM based round pin-fin heat sinks for thermal management of electronics: Effect of pin-fin diameter. *Int J Heat Mass Transf*, **117**, 861–872.
 47. Arshad, A., Ali, H.M., Ali, M., and Manzoor, S. (2017) Thermal performance of phase change material (PCM) based pin-finned heat sinks for electronics devices: Effect of pin thickness and PCM volume fraction. *Appl Therm Eng*, **112**, 143–155.
 48. Mahmoud, S., Tang, A., Toh, C., AL-Dadah, R., and Soo, S.L. (2013) Experimental investigation of inserts configurations and

- PCM type on the thermal performance of PCM based heat sinks. *Appl Energy*, **112**, 1349–1356.
49. Leong, K.Y., Chew, S.P., Gurunathan, B.A., Ku Ahmad, K.Z., and Ong, H.C. (2019) An experimental approach to investigate thermal performance of paraffin wax and 1-hexadecanol based heat sinks for cooling of electronic system. *International Communications in Heat and Mass Transfer*, **109**.
 50. Kumar, A., Kothari, R., Saxena, V., Sahu, S.K., and Kundalwal, S.I. (2022) Experimental investigation on paraffin wax-based heat sinks with cross plate fin arrangement for cooling of electronic components. *J Therm Anal Calorim*, **147** (17), 9487–9504.
 51. Pourhemmati, S., and Hossainpour, S. (2023) Thermal improvement of the vertical plate-fin heat sink by variable fin thickness pattern and utilizing phase change material: A numerical investigation. *J Energy Storage*, **59**.
 52. Nayak, K.C., Saha, S.K., Srinivasan, K., and Dutta, P. (2006) A numerical model for heat sinks with phase change materials and thermal conductivity enhancers. *Int J Heat Mass Transf*, **49** (11–12), 1833–1844.
 53. Jeon, D., and Byon, C. (2017) Thermal performance of plate fin heat sinks with dual-height fins subject to natural convection. *Int J Heat Mass Transf*, **113**, 1086–1092.
 54. Zhang, K., Li, M.J., Wang, F.L., and He, Y.L. (2020) Experimental and numerical investigation of natural convection heat transfer of W-type fin arrays. *Int J Heat Mass Transf*, **152**.
 55. Abbas, A., and Wang, C.C. (2020) Augmentation of natural convection heat sink via using displacement design. *Int J Heat Mass Transf*, **154**.
 56. Akula, R., Gopinath, A., Rangarajan, S., and Balaji, C. (2021) Experimental and numerical studies on heat transfer from a PCM based heat sink with baffles. *International Journal of Thermal Sciences*, **159**.
 57. Huang, X., Shi, C., Zhou, J., Lu, X., and Xu, G. (2019) Performance analysis and design optimization of heat pipe sink

with a variable height fin array under natural convection. *Appl Therm Eng*, **159**.

58. Arshad, A., Jabbal, M., and Yan, Y. (2020) Preparation and characteristics evaluation of mono and hybrid nano-enhanced phase change materials (NePCMs) for thermal management of microelectronics. *Energy Convers Manag*, **205**.
59. Zhang, L., Zhang, P., Wang, F., Kang, M., Li, R., Mou, Y., and Huang, Y. (2016) Phase change materials based on polyethylene glycol supported by graphene-based mesoporous silica sheets. *Appl Therm Eng*, **101**, 217–223.
60. Dinesh, R., Hussain, S.I., Roseline, A.A., and Kalaiselvam, S. (2021) Experimental investigation on heat transfer behavior of the novel ternary eutectic PCM embedded with MWCNT for thermal energy storage systems. *J Therm Anal Calorim*, **145** (6), 2935–2949.
61. Ravi Kumar, K., Balasubramanian, K.R., Jinshah, B.S., and Abhishek, N. (2022) Experimental Analysis and Neural Network Model of MWCNTs Enhanced Phase Change Materials. *Int J Thermophys*, **43** (1).
62. Murugan, P., Ganesh Kumar, P., Kumaresan, V., Meikandan, M., Malar Mohan, K., and Velraj, R. (2018) Thermal energy storage behaviour of nanoparticle enhanced PCM during freezing and melting. *Phase Transitions*, **91** (3), 254–270.
63. Ali, H.M. (2021) Analysis of heat pipe-aided graphene-oxide based nanoparticle-enhanced phase change material heat sink for passive cooling of electronic components. *J Therm Anal Calorim*, **146** (1), 277–286.
64. Yadav, C., and Sahoo, R.R. (2021) Thermal performance analysis of MWCNT-based capric acid PCM thermal energy storage system. *J Therm Anal Calorim*, **146** (4), 1539–1550.
65. Kumar, A., Kothari, R., Sahu, S.K., and Kundalwal, S.I. (2021) Thermal performance of heat sink using nano-enhanced phase change material (NePCM) for cooling of electronic components. *Microelectronics Reliability*, **121**.

66. Alimohammadi, M., Aghli, Y., Alavi, E.S., Sardarabadi, M., and Passandideh-Fard, M. (2017) Experimental investigation of the effects of using nano/phase change materials (NPCM) as coolant of electronic chipsets, under free and forced convection. *Appl Therm Eng*, **111**, 271–279.
67. Tariq, S.L., Ali, H.M., Akram, M.A., and Janjua, M.M. (2020) Experimental investigation on graphene based nanoparticles enhanced phase change materials (GbNePCMs) for thermal management of electronic equipment. *J Energy Storage*, **30**.
68. Krishna, J., Kishore, P.S., and Solomon, A.B. (2017) Heat pipe with nano enhanced-PCM for electronic cooling application. *Exp Therm Fluid Sci*, **81**, 84–92.
69. Arshad, A., Jabbar, M., Faraji, H., Talebizadehsardari, P., Bashir, M.A., and Yan, Y. (2021) Numerical study of nanocomposite phase change material-based heat sink for the passive cooling of electronic components. *Heat and Mass Transfer/Waerme- und Stoffuebertragung*.
70. Bondareva, N.S., Buonomo, B., Manca, O., and Sheremet, M.A. (2018) Heat transfer inside cooling system based on phase change material with alumina nanoparticles. *Appl Therm Eng*, **144**, 972–981.
71. Mahdi, J.M., and Nsofor, E.C. (2016) Solidification of a PCM with nanoparticles in triplex-tube thermal energy storage system. *Appl Therm Eng*, **108**, 596–604.
72. Hosseinizadeh, S.F., Darzi, A.A.R., and Tan, F.L. (2012) Numerical investigations of unconstrained melting of nano-enhanced phase change material (NEPCM) inside a spherical container. *International Journal of Thermal Sciences*, **51** (1), 77–83.
73. Kashani, S., Ranjbar, A.A., Madani, M.M., Mastiani, M., and Jalaly, H. (2013) Numerical study of solidification of a nano-enhanced phase change material (NEPCM) in a thermal storage system. *Journal of Applied Mechanics and Technical Physics*, **54** (5), 702–712.
74. Elbahjaoui, R., and El Qarnia, H. (2017) Thermal analysis of nanoparticle-enhanced phase change material solidification in a

- rectangular latent heat storage unit including natural convection. *Energy Build*, **153**, 1–17.
75. Sushobhan, B.R., and Kar, S.P. (2017) Thermal Modeling of Melting of Nano based Phase Change Material for Improvement of Thermal Energy Storage. *Energy Procedia*, **109**, 385–392.
 76. Faraji, H., Faraji, M., and El Alami, M. (2020) Numerical survey of the melting driven natural convection using generation heat source: Application to the passive cooling of electronics using nano-enhanced phase change material. *J Therm Sci Eng Appl*, **12** (2).
 77. Wu, S., Yan, T., Kuai, Z., and Pan, W. (2020) Experimental and numerical study of modified expanded graphite/hydrated salt phase change material for solar energy storage. *Solar Energy*, **205**, 474–486.
 78. Wu, J., Feng, Y., Liu, C., and Li, H. (2018) Heat transfer characteristics of an expanded graphite/paraffin PCM-heat exchanger used in an instantaneous heat pump water heater. *Appl Therm Eng*, **142**, 644–655.
 79. Ren, Q., Guo, P., and Zhu, J. (2020) Thermal management of electronic devices using pin-fin based cascade microencapsulated PCM/expanded graphite composite. *Int J Heat Mass Transf*, **149**.
 80. Lin, W., Ling, Z., Zhang, Z., and Fang, X. (2020) Experimental and numerical investigation of sebacic acid/expanded graphite composite phase change material in a double-spiral coiled heat exchanger. *J Energy Storage*, **32**.
 81. Huang, Z., Gao, X., Xu, T., Fang, Y., and Zhang, Z. (2014) Thermal property measurement and heat storage analysis of LiNO₃/KCl - expanded graphite composite phase change material. *Appl Energy*, **115**, 265–271.
 82. Lv, Y., Zhou, W., and Jin, W. (2016) Experimental and numerical study on thermal energy storage of polyethylene glycol/expanded graphite composite phase change material. *Energy Build*, **111**, 242–252.
 83. Ma, C., Zhang, Y., Chen, X., Song, X., and Tang, K. (2020) Experimental study of an enhanced phase change material of

- paraffin/expanded graphite/nano-metal particles for a personal cooling system. *Materials*, **13** (4).
84. Cai, W., He, F., Zhang, Q., Li, Y., Zhou, Y., Yang, Z., He, R., Zhang, K., and Yang, W. (2020) Experimental and numerical simulation of phase change process for paraffin/expanded graphite/ethylene-vinyl acetate ternary composite. *Appl Therm Eng*, **169**.
 85. Akula, R., and Balaji, C. (2022) Thermal management of 18650 Li-ion battery using novel fins-PCM-EG composite heat sinks. *Appl Energy*, **316**.
 86. Zhang, Z., Zhang, N., Peng, J., Fang, X., Gao, X., and Fang, Y. (2012) Preparation and thermal energy storage properties of paraffin/expanded graphite composite phase change material. *Appl Energy*, **91** (1), 426–431.
 87. Cai, W., Yang, W., Jiang, Z., He, F., Zhang, K., He, R., Wu, J., and Fan, J. (2019) Numerical and experimental study of paraffin/expanded graphite phase change materials with an anisotropic model. *Solar Energy Materials and Solar Cells*, **194**, 111–120.
 88. Akgün, H., Yapıcı, E., Özkan, A., Günkaya, Z., and Banar, M. (2023) A combined multi-criteria decision-making approach for the selection of carbon-based nanomaterials in phase change materials. *J Energy Storage*, **60**.
 89. Wang, C., Cai, Z., Chen, K., Huang, J., and Wang, T. (2019) Preparation and thermal properties of shape-stabilized polyethylene glycol/mesoporous silica composite phase change materials for thermal energy storage. *Energy Storage*, **1** (2), e45.
 90. Ji, J., Wang, Y., Lin, X., Liu, B., and Zhang, X. (2021) Fabrication of highly thermal conductive and shape-stabilized phase change materials. *J Energy Storage*, **44**.
 91. Wang, C., Chen, K., Huang, Z., Wang, T., and Chen, F. (2020) Effect of polymer-derived silicon carbonitride on thermal performances of polyethylene glycol based composite phase change materials. *Solar Energy*, **208**, 282–288.

92. Ye, G., Zhang, G., Jiang, L., and Yang, X. (2022) Temperature control of battery modules through composite phase change materials with dual operating temperature regions. *Chemical Engineering Journal*, **449**.
93. Tariq, S.L., Ali, H.M., Akram, M.A., Janjua, M.M., and Ahmadlouydarab, M. (2020) Nanoparticles enhanced phase change materials (NePCMs)-A recent review. *Appl Therm Eng*, **176**.
94. Jilte, R., Afzal, A., and Panchal, S. (2021) A novel battery thermal management system using nano-enhanced phase change materials. *Energy*, **219**.
95. Kothari, R., Sahu, S.K., and Kundalwal, S.I. (2021) Investigation on thermal characteristics of nano enhanced phase change material based finned and unfinned heat sinks for thermal management system. *Chemical Engineering and Processing - Process Intensification*, **162**.
96. Kothari, R., Sahu, S.K., Kundalwal, S.I., and Mahalkar, P. (2021) Thermal performance of phase change material-based heat sink for passive cooling of electronic components: An experimental study. *Int J Energy Res*, **45** (4), 5939–5963.
97. Coleman, H.W., and Steele, W.G. *Experimentation, validation, and uncertainty analysis for engineers*.
98. Effendi, N.S., and Kim, K.J. (2017) Orientation effects on natural convective performance of hybrid fin heat sinks. *Appl Therm Eng*, **123**, 527–536.
99. Amudhalapalli, G.K., and Devanuri, J.K. (2022) Synthesis, characterization, thermophysical properties, stability and applications of nanoparticle enhanced phase change materials – A comprehensive review. *Thermal Science and Engineering Progress*, **28**.
100. Rehman, T. ur, and Ali, H.M. (2020) Experimental study on the thermal behavior of RT-35HC paraffin within copper and Iron-Nickel open cell foams: Energy storage for thermal management of electronics. *Int J Heat Mass Transf*, **146**.

101. Baby, R., and Balaji, C. (2013) Thermal optimization of PCM based pin fin heat sinks: An experimental study. *Appl Therm Eng*, **54** (1), 65–77.
102. Huang, Y., Sun, Q., Yao, F., and Zhang, C. (2021) Experimental Study on the Thermal Performance of a Finned Metal Foam Heat Sink with Phase Change Material. *Heat Transfer Engineering*, **42** (7), 579–591.